Journal of Alloys and Compounds 509 (2011) 4214–4234

Contents lists available at ScienceDirect

Journal of Alloys and Compounds

journal homepage: www.elsevier.com/locate/jallcom

Density functional study of AlB_n clusters for $n = 1–14$

Mustafa Böyükata [a,*], Ziya B. Güvenç [b]

[a] Department of Physics, Bozok University, 66200 Yozgat, Turkey
[b] Department of Electronic and Communication Engineering, Çankaya University, 06530 Ankara, Turkey

ARTICLE INFO

Article history:
Received 28 October 2010
Received in revised form
31 December 2010
Accepted 9 January 2011
Available online 14 January 2011

Keywords:
Aluminum
Boron
Density functional theory
Cluster

ABSTRACT

Density functional theory (DFT) B3LYP at 6-311++G(d,p) level is employed to optimize the structures of AlB_n ($n = 1–14$) microclusters. Analysis of the energetic and structural stability of these clusters and their various isomers are presented. Total and binding energies of the clusters have been calculated. Their harmonic frequencies, point symmetries, and the highest occupied molecular orbital-lowest unoccupied molecular orbital (HOMO–LUMO) energy gaps have been determined. Results are evaluated by comparing to the previous similar works.

1. Introduction

Studies on clusters (as an intermediate state of the matter between atoms/molecules and bulk) are quite important for the future of nanotechnological applications. Their exotic properties, different from their bulk phase and size dependence, have caused considerable attention [1–32]. Their unusual physical and chemical properties such as structural, electronic, and thermodynamics are not well understood and, as a result, they are still the subjects of intense research. One of the important preliminary steps towards the possible use of nanoclusters is the understanding of the intricate connection between the atomic and electronic structures. Unfortunately, determinations of the equilibrium structures and of the atomic arrangements in the clusters have not yet been generalized. Moreover, investigation and the production of isolated microclusters via experimental studies are extremely difficult. Computational simulations for predicting the cluster properties have been regarded as powerful tools and support the experimental studies. Such studies provide helpful atomistic level simulations by using ab initio methods, or the density functional theory (DFT) [7,8]. Despite the difficulty of determining the lowest-energy structure of a cluster containing more than 10 atoms, because of the high computation time, the electronic structure methods provide accurate results.

Boron and aluminum, as members of group-13 elements, are interesting and important in the physics and chemistry of nanoclusters and their alloys because of their useful potential in designing nanoscopic devices and catalysts. For a better understanding of these atomic aggregates, the small aluminum clusters have been extensively studied [9,10]. In some resent studies, for example, melting, crystallization, and local atomic arrangements of Al clusters have been investigated by using a reactive force field based on DFT [11]. Structures and stabilities of the putative global minima of 13- to 34-atom Al clusters with their ionic and cationic forms have been studied with first principles DFT [12]. Boron is the unique semimetallic one in that group and has high electro negativity and ionization energy properties like nonmetallic carbon. Boron is an electron-deficient semimetal and has a short covalent radius. Because of its high melting point and hardness it has been the subject of many studies [13–20]. Depending on the synthesis condition and the amount of boron, it has the ability to influence the structure and phase composition of materials [13,14]. General results for pure, small sized boron clusters show that the relatively more stable structures are, mainly, the planar and quasi-planar nuclear arrangements compared to any of the three-dimensional forms. There are also considerable interests in studying molecular or atomic species hosted by boron rich clusters. For example, in the literature, boron oxides [21], hydrogenated boron [22–24] and aluminum [25–27] clusters have been extensively studied.

Moreover, there is increasing attention on the growth pattern and electronic properties of metallic atom-doped boron clusters due to the practical values of metal-boron systems in many fields. Some of them, for instance, are the reports of the detailed investiga-

* Corresponding author. Tel.: +90 354 2421021/2581; fax: +90 354 2421022.
E-mail addresses: mustafa.boyukata@bozok.edu.tr, boyukata@yahoo.com (M. Böyükata), guvenc@cankaya.edu.tr (Z.B. Güvenç).

0925-8388/$ – see front matter © 2011 Elsevier B.V. All rights reserved.
doi:10.1016/j.jallcom.2011.01.053

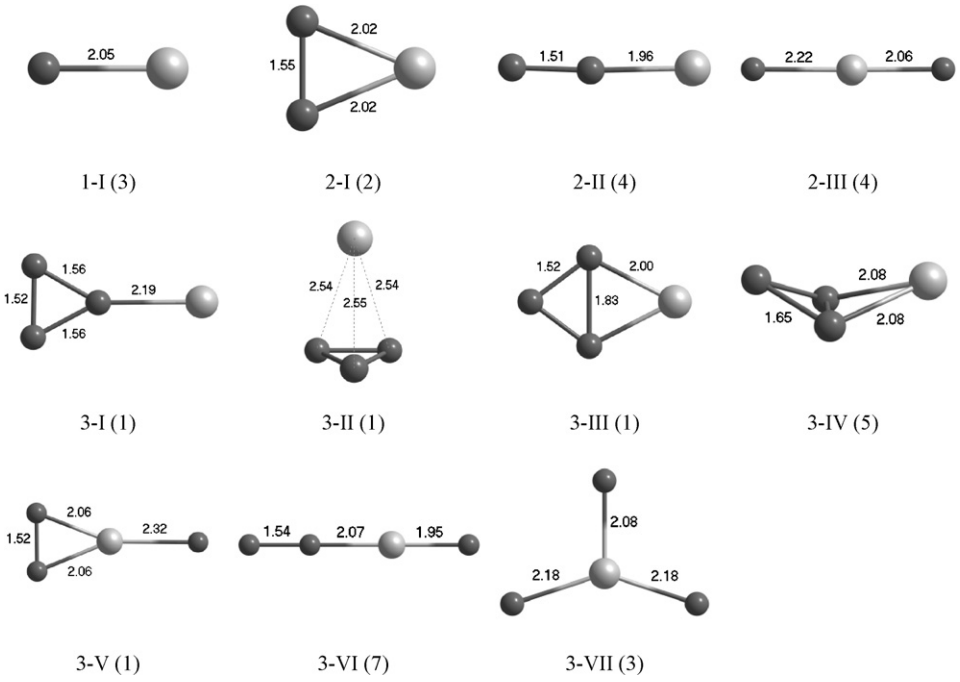

Fig. 1. Structures of AlB_n ($n = 1–3$) clusters.

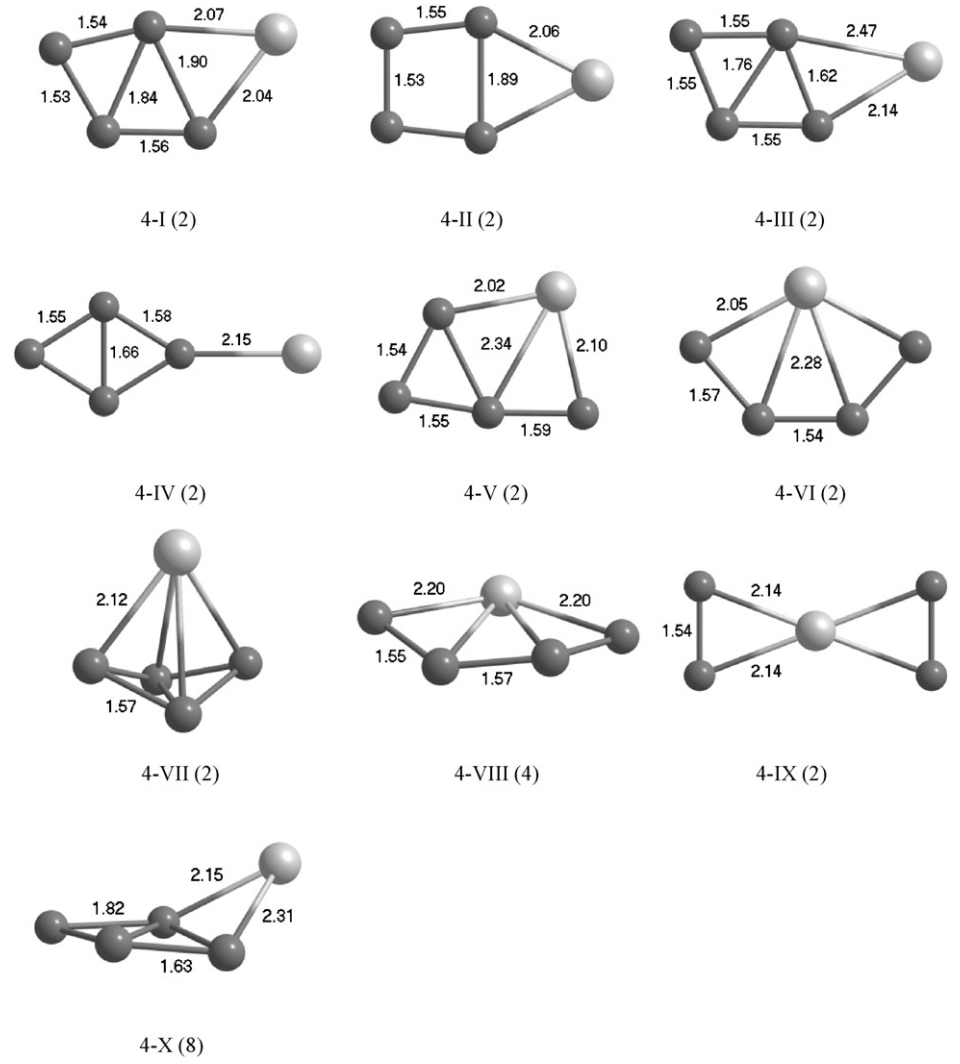

Fig. 2. Structures of AlB_4 clusters.

tion of B_7Au_2 with its ionic case [28], DFT study with the generalized gradient approximation (GGA) for the structure and magnetism of FeB_n (up to $n=6$) clusters [29], DFT study of Ni_nB (for $n=1$–8, 12) clusters [30], the theoretical interpretation of the structural stability of ZrB_n (up to $n=12$) clusters [31]. Another examples are findings of the change of the magnetic moment of Cr, Mn, Fe, Co and Ni doped B_n clusters (up to $n=7$) [32] and DFT results in the structure and stability of Al-doped Boron AlB_n (up to $n=12$) clusters [18]. The existing research on Al and B clusters has mainly focused on the structural and electronic properties [18]. Results of the AlB_n clusters are different from the encapsulation of a transition metal into the B clusters because a transition metal atom has the unfilled 3d subshell. Despite the existing study of Al-doped boron clusters [18], there is a lack of systematic reporting on their growth behaviors as well as the electronic properties in relation to the increasing size of the clusters. Hence, it is necessary to investigate further various structural isomers of the Al doped B clusters and to provide detailed information about the influences of the same group metal atom and different functionals.

In this work, DFT-B3LYP at 6-311++G(d,p) [33] level is employed via the Gaussian program [33] to optimize the structures of the AlB_n ($n=1$–14) microclusters. The analysis of the energetic and structural stability of these clusters depends on the various isomers that are presented. The total and binding energies of the clusters have been calculated. Their harmonic frequencies, point symmetries, and the HOMO–LUMO energy gaps have been determined. Results are evaluated with respect to previous similar works [18,29,31]. This work is meant to improve the basic understanding of the growth sequence of these microclusters, which follows a similar approach in regards to the previous work on boron [20] clusters. DFT simulations have been performed using the same functional and basis set for boron hydrides [22–24]. The goals of this study are to establish an efficient optimization method and provide further understanding of the structural implications of this approach by identifying the characteristic structural motifs associated with the stable minima of AlB_n clusters. In particular, a possible geometrical packing phenomenon was studied for $n=1$–14 sizes. This comprehensive study would fill the gap in the literature of the aluminum–boron clusters by investigating systematically more of their structures, and scanning much larger isomer-space of the corresponding sizes. As a result, we have obtained many more lower-lying and energetically higher isomers of the studied AlB_n clusters. In addition, analysis of all these structures of the AlB_n clusters is made by calculating more of their physical quantities (they are explained in the text, respectively) than those already published in the literature [18]. Therefore this work has a good addition to the previous publications in this field, and may be quite useful for the future studies on the same subject.

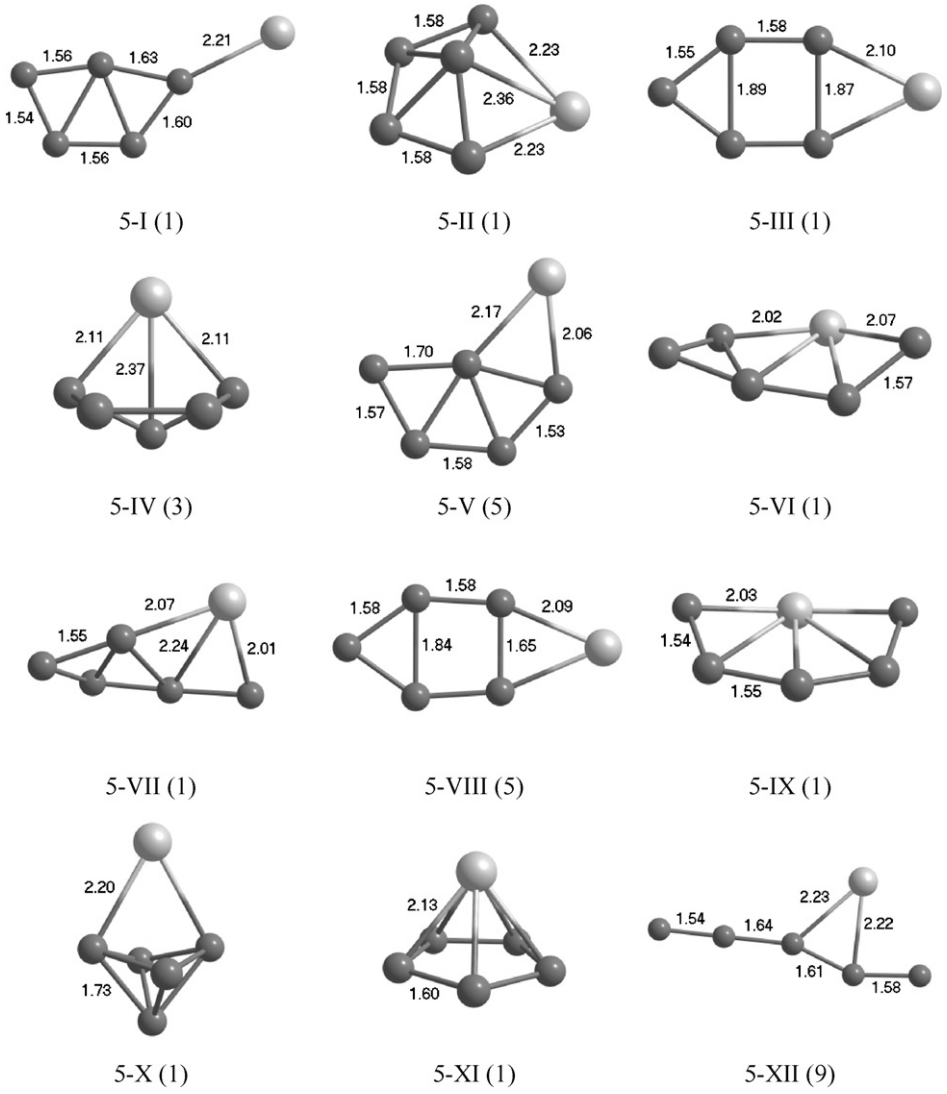

Fig. 3. Structures of AlB_5 clusters.

2. Theoretical background

The DFT has been employed to carry out the geometry optimization of the AlB_n ($n = 1–14$) microclusters. The approach adopted in this work has been previously described elsewhere [22–24]. Briefly, in the electronic structure calculations, the theory of B3LYP functional was treated with the basis at 6-311++G(d,p) level in Gaussian package [33]. Reliability of the selected method for the present calculations has been shown via using it for pure boron clusters [20] and their hydrides [22–24]. To determine the ground-state (G-S) isomers, after geometry optimization, the total energies were compared between the same sized clusters.

In order to see the structural stability of the AlB_n clusters the energetic analysis has been carried out for the various isomers with the following formula. For the total binding energies of the clusters:

$$E_b = E[AlB_n] - (nE[B] + E[Al]) \quad (1)$$

is used in which the $E[B]$ (−671.105 eV) and $E[Al]$ (−6595.722 eV) are the energies of a single boron and single aluminum atom with the zero-point-energy (ZPE) corrections, respectively. The average binding energies per atom can be obtained from $E_b[AlB_n]/(n+1)$. The number n is the number of boron atoms. The dissociation energies of B and Al atoms in the clusters are written as:

$$E_{dB}(n) = E[AlB_n] - (E[AlB_{n-1}] + E[B]) \quad (2)$$

$$E_{dAl}(n) = E[AlB_n] - (E[B_n] + E[Al]) \quad (3)$$

The second finite difference of the optimized clusters is calculated from:

$$\Delta_2 E = E[AlB_{n+1}] + E[AlB_{n-1}] - 2E[AlB_n] \quad (4)$$

as a function of the number of boron atoms. Their harmonic frequencies, point symmetries, and HOMO–LUMO energy gaps have been determined.

3. Results and discussion

The number of isomers of the AlB_n clusters for $n = 1–14$ have been systematically obtained by employing the described computational scheme of DFT/B3LYP/6-311++G(d,p). The predicted G-S structures and various low-lying metastable isomers are shown in Figs. 1–12. Determination of the isomers is based on the compar-

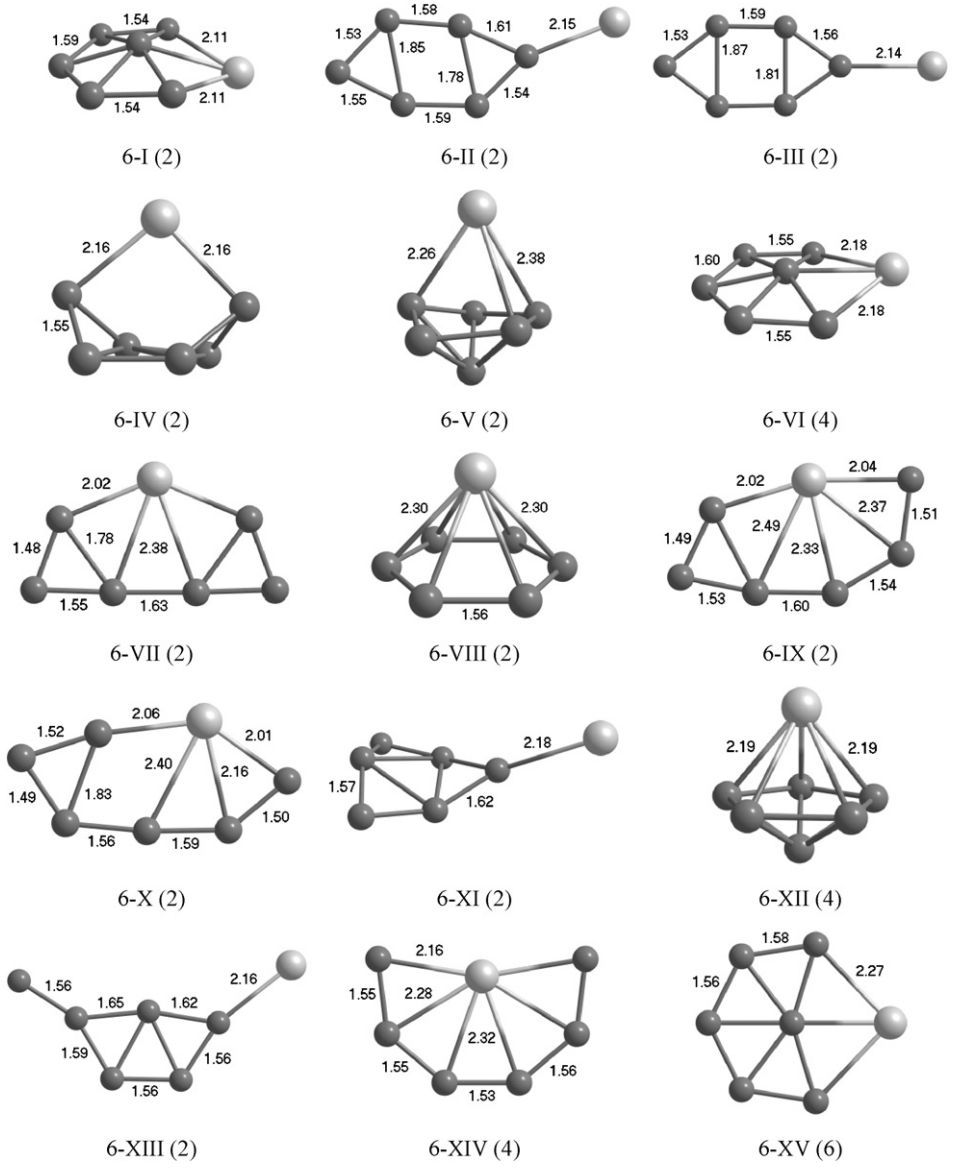

Fig. 4. Structures of AlB_6 clusters.

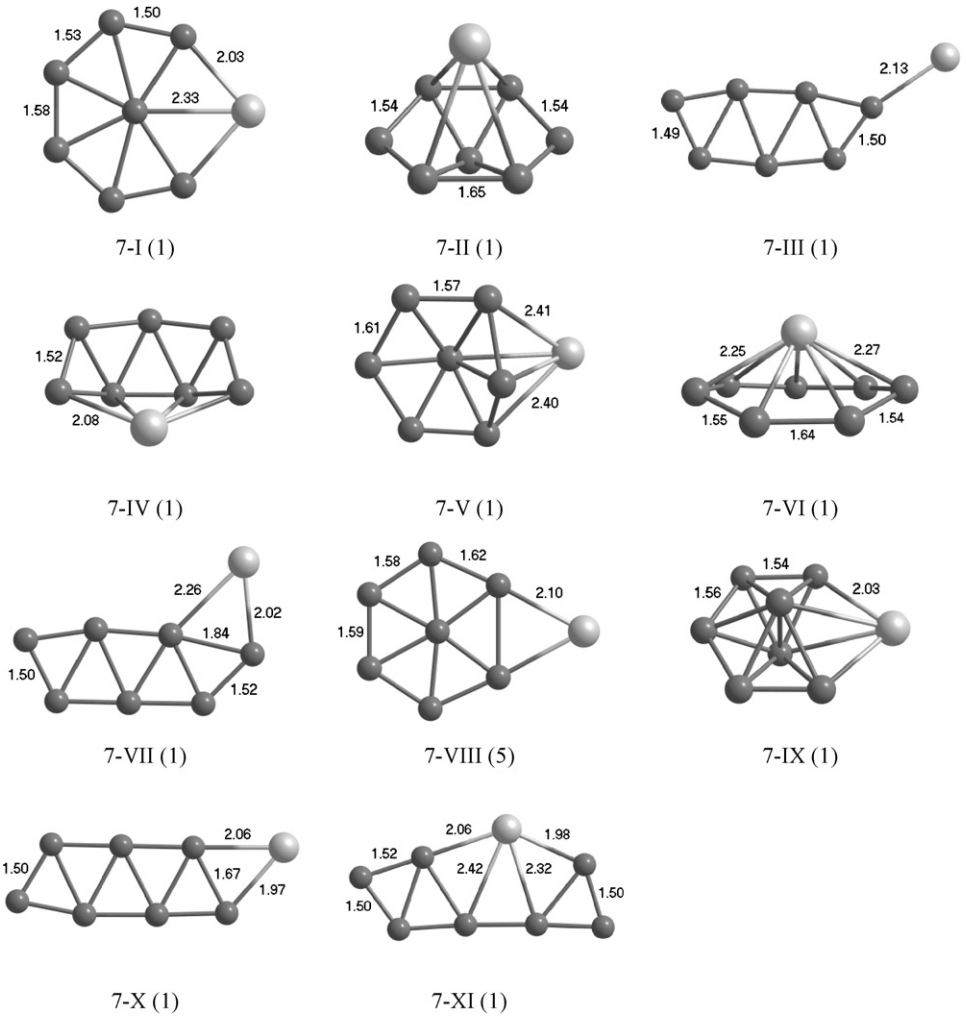

Fig. 5. Structures of AlB_7 clusters.

ison of their total energies. The calculated values of the total and binding energies, the harmonic frequencies, the point symmetries, and the HOMO–LUMO energy gaps are listed in Table 1. The energy values have been computed with the ZPE corrections in the present work. However, relative energies (ΔE) given in Table 1 are different than those of Ref. [18] for the common isomers. In order to find out the source of this difference (since the code used, and the DFT functional in both studies are the same, and the basis sets are the same) we have removed the ZPE effects from our energy differences. We observed mainly the same or reasonably closer ΔE values with the values of Ref. [18] for the common isomers. This shows that in Ref. [18] the energy values do not include the ZPE corrections. This correction may have a significant effect on the order of the isomers. Therefore, the ZPE correction should be included for the isomer search.

In Fig. 1, the putative structures for AlB_n ($n = 1$–3) clusters are seen within energetical order from the lowest to the highest energy values. For the AlB dimer with $C_{\infty v}$ symmetry, the results indicate that the total energy of the triplet AlB is lower than those of the singlet and quintet states by 0.918 and 1.190 eV, respectively. Bond-length of the triplet Al–B (2.05 Å) is longer than that of the quintet Al–B (1.94 Å) and shorter than that of the singlet Al–B (2.09 Å). Hence, the most stable triplet AlB dimmer should be regarded as the G-S. All of the calculated G-S structures from $n = 2$ to $n = 14$ correspond to the singlet and doublet states for the odd and even number of boron atoms in the clusters, respectively. There are three structural isomers for AlB_2 clusters in the figure. The most stable one is in an isosceles (C_{2v}) triangular shape of the doublet AlB_2. The others are quartets and in one-dimensional (1D) forms. The last one has the Al atom between the two boron atoms. These geometries have been examined for various multiplicities (doublet, quartet, sextet and octet). Their energetics and structural parameters are not given here. In brief, the quartet of the first isomer has the second lowest energy. The sextet and doublet states of the isomer 2-II and the sextet of the isomer 2-I are between the second and third isomers, respectively. Finally, the isomers with the spin octet states follow the other geometries with the spin doublet and sextet states of the third isomer, respectively. The most stable of the AlB_3 clusters is the singlet two-dimensional (2D) planar form as the Al is bonding with one B atom of the triangular B_3 cluster, constructing a Y-like structure. The three-dimensional (3D) one is the second low-lying isomer, in which the Al atom sits on the hallow site of triangular borons and causes a pyramidal structure. With two-coordination numbers the Al makes a planar close packing form in the isomer 3-III (Al caps the peripheral site of the triangular B_3 frame) and it is banding with the increasing spin states of the quintet rhombic geometry (isomer 3-IV) and septet (not given here). Similar to AlB_2 structures, keeping the Al atom between the B atoms does not make AlB_3 cluster more stable. An Al centered Y-like structure is the fifth low-lying isomer, 3-V in Fig. 1. The isomers 3-VI (1D septet, ^7A, $C_{\infty v}$) and 3-VII (2D triplet, ^3A, C_s) are less stable isomers in the series. Moreover, isomer 3-II has been analyzed with various spin multiplet states but they

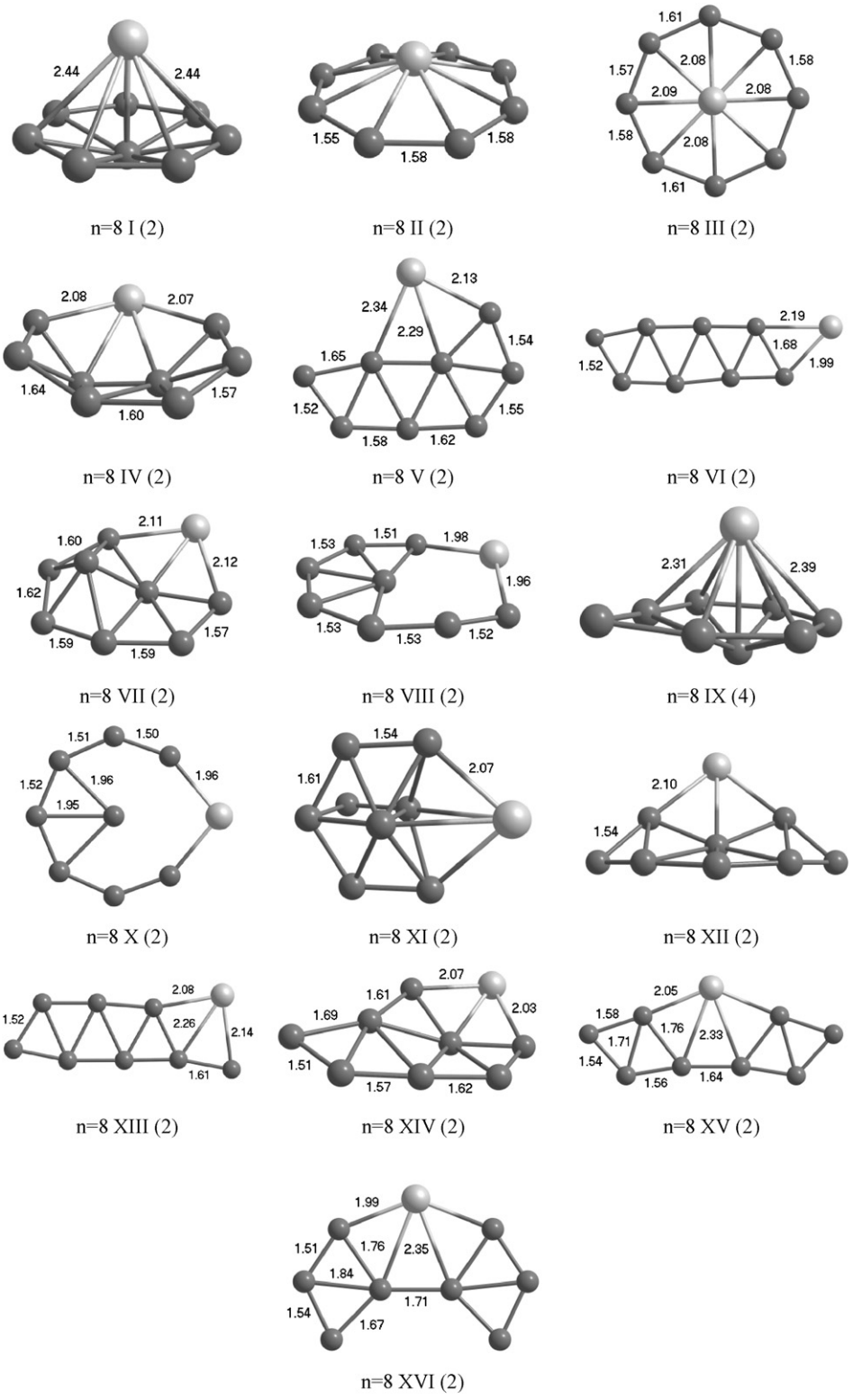

Fig. 6. Structures of AlB_8 clusters.

are not stable. For example, its nonet state has been obtained with a bond-length of Al–B, 2.13 Å, which is the least stable isomer (not given here). The boron structures in the G-S forms are very similar to those of the G-S structures of bare boron clusters. Simply, the Al atom attaches itself to those G-S bare boron clusters.

The observed structures of the AlB_4 clusters are shown in Fig. 2. Mainly, relatively more stable structures are in planar orientation and not keeping the Al atom inside of the boron atoms. In the G-S structure, that grows from 3-III, the Al atom is placed on the peripheral site of the 4-atom boron cluster with C_s symmetry, which is a close-shell form of the substitutional structure of W-like geometry with little distortion. In Ref. [18] the same geometry has been reported as the lowest energy structure and two more isomers corresponding to our third (C_s) and sixth (C_{2v}) isomers within the

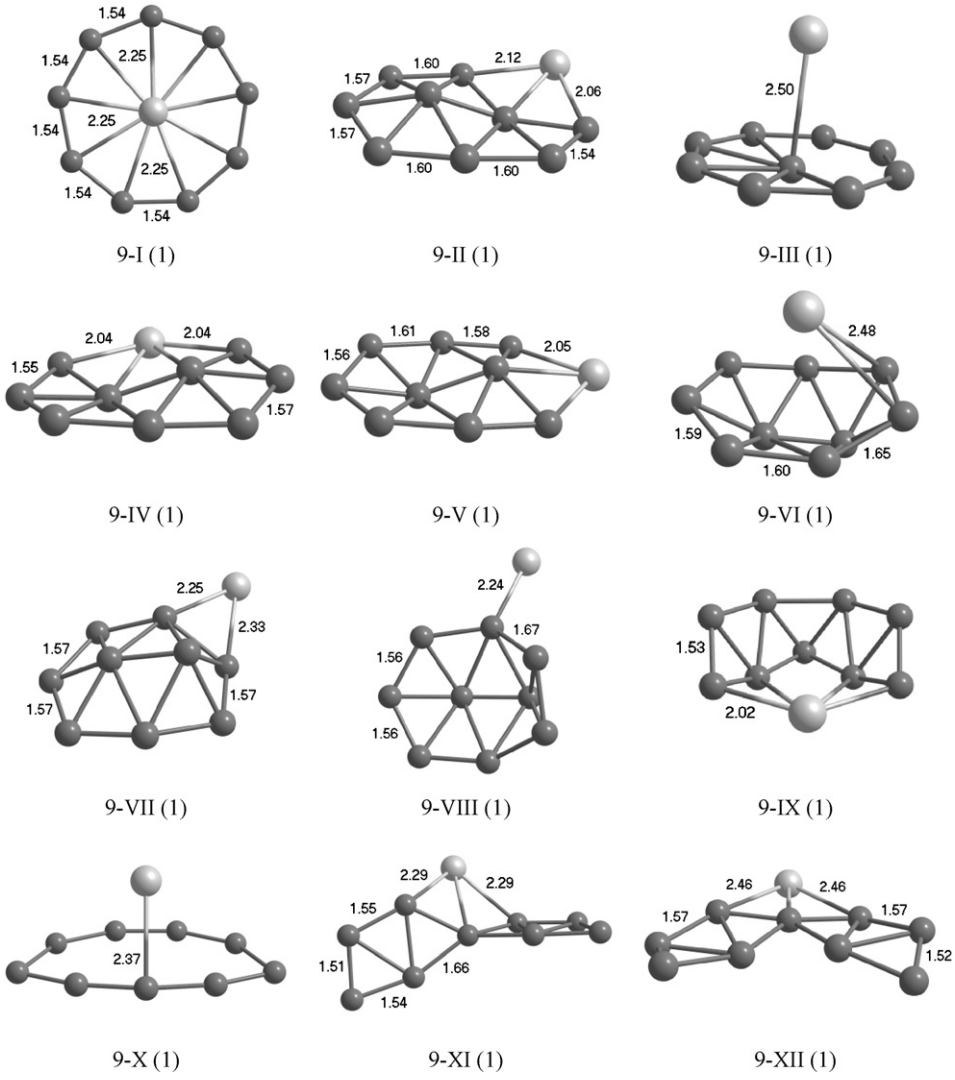

Fig. 7. Structures of AlB_9 clusters.

energy interval of 0.924 eV are reported as well. However, here, the first six isomers are in 0.907 eV. We obtained a second isomer in which the Al atom was added to one of the peripheral sites of the square-like structure of a 4-boron atom having a little distortion. Isomer 4-IV (Al on atop-site of one of the boron atoms) and isomer 4-V (having Al with the coordination number 3) are energetically more stable than the third isomer of Ref. [18]. In Ref. [18] no pyramidal structure of AlB_4 was reported. However, we obtained a capped trigonal pyramidal structure (isomer 4-VII) out of the energy interval, 1.154 eV above the lowest-energy structure. Putting the Al atom between the boron atoms, in B_4, results in a less stable X-like structure (isomer 4-IX). Moreover, less stable isomers are obtained by increasing the spin multiplicity (isomers 4-VIII and 4-X), which are substantially higher in energy.

Fig. 3 gives the optimized geometries for $n = 5$. The G-S structure AlB_5 with C_s symmetry grows from the isomer 4-IV of AlB_4 by adding one B atom. It forms a W-like geometry of B_5. The first two isomers are in agreement with the results obtained in Ref. [18]. The singlet kite-like structure (5-IX) is not a G-S structure even though the Al atom is coordinated with all 5 boron atoms. There are six isomers within 2.763 eV of an energy interval in Ref. [18]. Up to the pentagonal pyramidal isomer, 5-XI, in Fig. 3 the structures found here are in an energy interval of 2.738 eV. One more isomer out of this interval was also obtained with a spin multiplicity of 9 in which the boron atoms have a line-like shape (isomer 5-XII). Isomer 5-I has been recalculated with a spin triplet state (not given here) and is energetically not lower than isomer 5-I, which is between isomers 5-II and 5-III. Moreover, in isomer 5-V the Al atom prefers to sit on the bridge site of the W-like structure of B_5 with a spin multiplicity of 5. It has also been analyzed with a spin 7 but it is energetically less stable, between the isomers 5-XI and 5-XII.

As seen in Fig. 4 the G-S structure for $n = 6$ is in doublet quasiplanar configuration (closer to planar form, an Al-membered hexagon capped by a boron atom at the center) which grows from the 5-II. Fifteen geometries within the energy interval of 2.543 eV have been considered for the AlB_6 cluster. In Ref. [18] just 3 isomers in three-dimensional form have been reported within a relatively large energy interval of 7.194 eV. Those three isomers in Ref. [18] correspond to isomers 6-V (distorted pentagonal bipyramid), 6-VIII (heptagonal pyramid) and 6-XII (pentagonal bipyramid) in Fig. 4, respectively. This comparison and our results show that the G-S structure for the AlB_6 is in a quasiplanar form, not in 3D as pointed out in Ref. [18]. The newly found 3D structure (6-IV) is also one of the lower-lying of those three 3D clusters. Our second and third most stable isomers are also in 2D geometries. The quartet isomer 6-XIV (Al-centered with 6-boron coordinated structure of kit-like geometry) and the sextet isomer 6-XV (planar

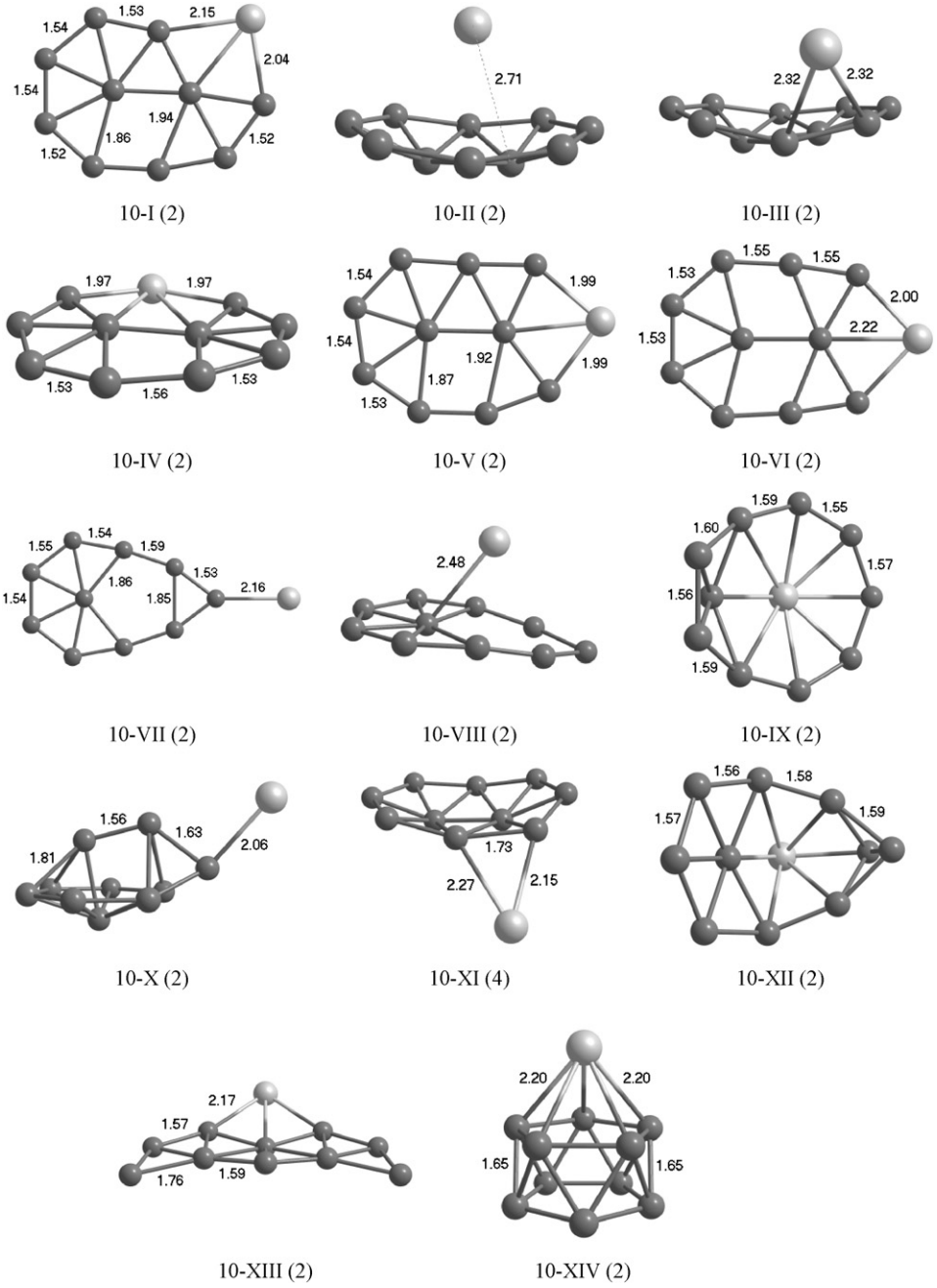

Fig. 8. Structures of AlB_{10} clusters.

Al-membered hexagon capped by one-boron at the center) are the least stable configurations of the AlB_6 clusters.

Eleven isomers between the G-S and the least stable local minima within the energy interval of 1.294 eV for AlB_7 cluster are shown in Fig. 5. The G-S isomer, growing from 6-XV, is in a planar form in which one B atom is centered and six atoms (Al-membered heptagon) are around it. This geometry was not obtained in the previous work [18]. The pyramidal structures, 7-II, -VI and -IX (hexagonal bipyramid having Al over the hexagonal ring, heptagonal pyramid and hexagonal bipyramid having Al-membered hexagonal ring), are not lower than 7-I. Moreover, without ZPE correction 7-IV is energetically lower-lying than 7-III. In Ref. [18] four isomers have been obtained within the energy interval of 1.387 eV. Their structural morphology looks like the isomers 7-II, 7-XI, 7-VI and 7-IX in Fig. 5, respectively. Their second most stable isomer is here the least stable one, 7-XI.

The structural characterization of AlB_8 is given in Fig. 6 with 18 obtained isomers in the energy interval of 2.868 eV. Various planar structures were performed to find any low-lying isomers. However, the G-S isomer growing from 7-VI is in 3D configuration, like an umbrella (distorted heptagonal bipyramid or dimmer surrounded by seven boron atoms). This is in agreement with the previous work [18]. Isomer 8-II is like an octagonal pyramid since the Al atom is slightly over the 8-boron ring plane. In Ref. [18] two structures are reported and the second one is energetically 1.452 eV higher than the lowest one that corresponds to our third isomer, 1.406 eV higher than the G-S one. Isomer 8-III, octagon with a central Al atom, is the first structure fully constructed boron ring around the Al atom, which is a wheel planar structure. Exchanging Al with any boron atom of the ring in 8-III leads to isomer 8-X. Close packaging 3D geometries quartet 8-IX (boron capped hexagonal bipyramid) and doublet 8-XI (Al capped distorted trigo-

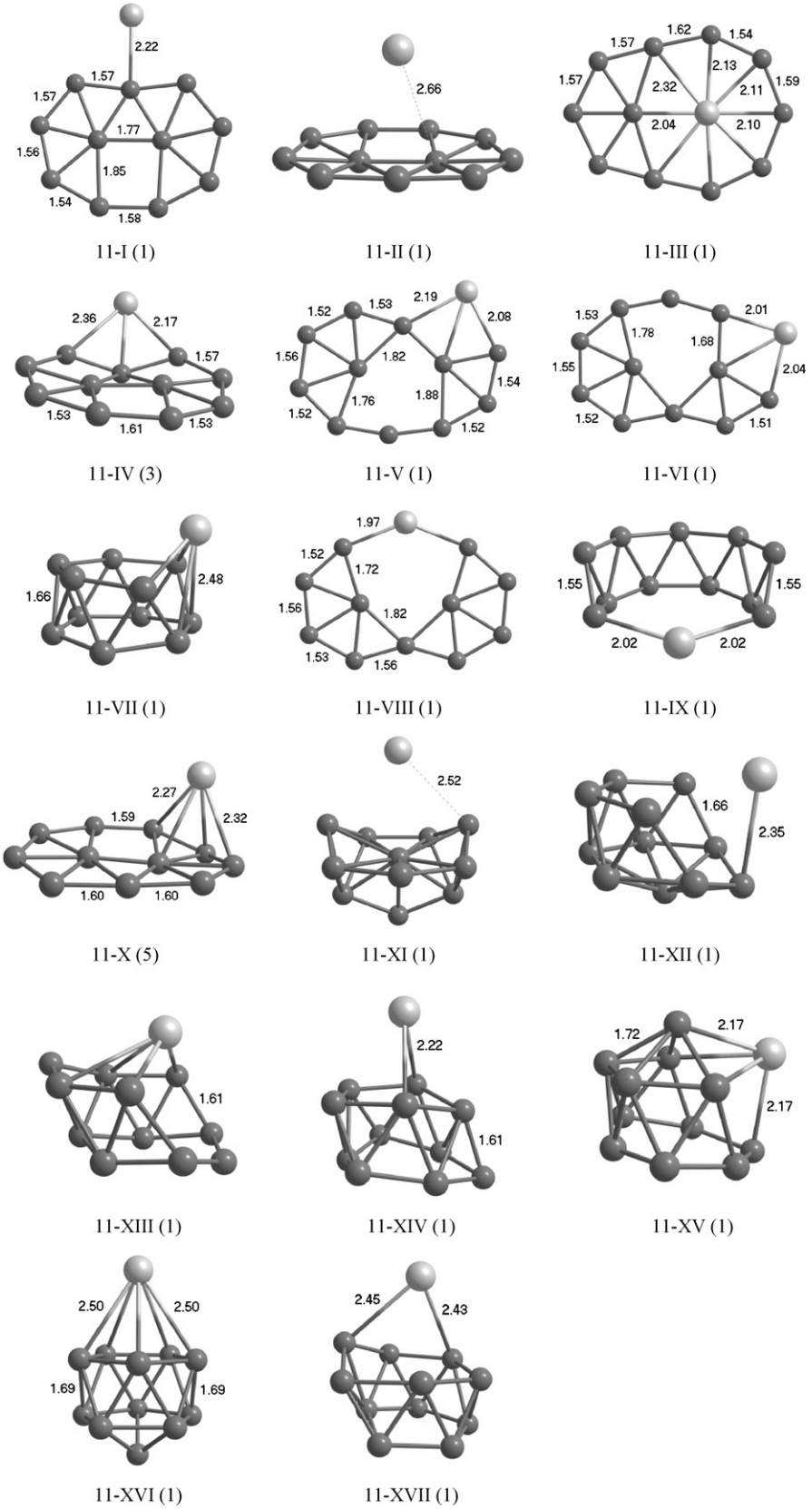

Fig. 9. Structures of AlB_{11} clusters.

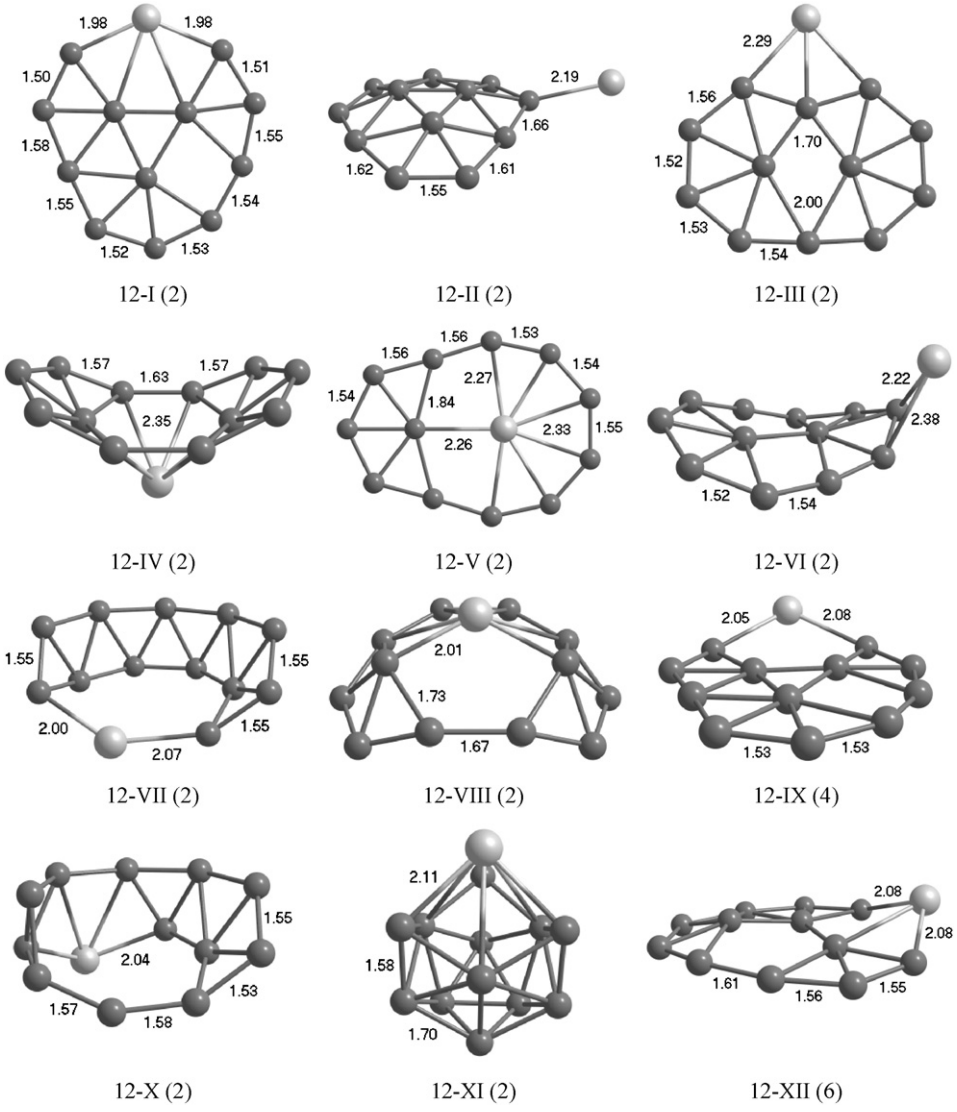

Fig. 10. Structures of AlB_{12} clusters.

nal biprism) are also energetically much higher than the obtained G-S one.

Interestingly, for $n = 9$ the singlet nonagon with a central Al atom the G-S isomer is in a planar wheel structure for AlB_9, as seen in Fig. 7. It looks like it is growing from 8-III. In the energy interval of 3.691 eV twelve isomers for the $n = 9$ are given here. However, only three isomers were reported in Ref. [18] within 2.763 eV, similar to the isomers of 9-III (umbrella-like), 9-V (dovetailed hexagonal bipyramid) and 9-X (distorted and open caged nonagonal pyramid), respectively. Two different configurations of the two dovetailed hexagonal pyramids like geometry of 9-V have been recalculated and we obtained energetically lower isomers, 9-II and IV. With a spin multiplicity of 5, the G-S isomer of AlB_9 is also stable, yet the least stable isomer. It is even less stable than isomer 9-XII and, therefore, not given here.

Arrangement of the atoms in the G-S structure of AlB_{10}, as seen in Fig. 8, is a planar form growing from the 9-II. One distorted heptagonal pyramid and one Al-membered hexagonal pyramid make up the subunits in the G-S doublet isomer, 10-I. Fourteen isomers are presented here. Our G-S isomer was reported as the second one in Ref. [18] since we considered the ZPE correction. We obtained their first stable structure as the second isomer 10-II, in which Al sits over the nearly flat B_{10} having 2-hexagonal pyramids as subunits. Hence, it is observed that the 2D-structure for the AlB_{10} is more stable than 3D. The third isomer (0.988 eV higher than the most stable isomer) of Ref. [18] is similar to 10-VIII (0.952 eV higher than the G-S structure). Additionally, the G-S structure has been computed with quartet multiplicity (not given here) which almost stays in the same configuration and it is energetically between 10-IX and 10-X.

The G-S structure of AlB_{11} is in a planar form, Al attached to atop-site of one boron atom in the complex as seen in Fig. 9. It grows via replacing a boron atom with the Al atom in 10-IV, putting the Al atom on atop-site of the replaced boron. The second low-lying isomer 11-II (0.700 eV higher than the G-S) is in 3D configuration which is the G-S structure of Ref. [18]. In Ref. [18] the second stable structure 1.377 eV higher than their most stable isomer which corresponds to our 11-VI isomer, i.e., the corresponding energy difference between 11-II and 11-VI is 1.371 eV. Moreover, isomer 11-VI is 2.071 eV higher than the present most stable structure. There are in total five different structures within the energy interval of 3.246 eV for $n = 11$ in Ref. [18]. The last three of them are in 3D form and contain double ring–like configurations of atoms. We have also analyzed, in detail, similar isomers within an energy interval of 3.94 eV. The 3D structures are clearly less stable than 2D configurations. Cage form of the AlB_{11} (11-XVI) is obviously seen as one of the least stable structures of the group of this size.

Determined structures for AlB_{12} are illustrated in Fig. 10. In a planar form of the G-S structure, a triangular B_3 is surrounded by 9-boron atoms and the Al atom is attached with a 4 coordination number. Previously three isomers in 3D form were reported in an energy interval of 1.863 eV for $n = 12$ [18]. In our case they correspond to 12-IV, 12-VII and 12-X, which are in 1.806 eV difference. In Ref. [18] the G-S structure is in a bowl-like geometry as 12-IV. In the present work twelve isomers are optimized within 3.770 eV. Mainly the 2D or semi-planar configurations are relatively more stable. The first 3 most stable isomers presented are not in 3D configurations. The Al atom in 12-II is attached to the B_{12} quasi planar form which has 3-hexagonal pyramids as subunits. The 12-II cluster without the ZPE correction becomes the most stable isomer. Capping the Al atom has 3-coordination with boron atoms in 12-III, in which the B_{12} surface has two B-centered heptagonal rings as subunits. The cage structure of 12-XI is one of the least stable isomers. Increasing the spin multiplicity results in the least stable isomer with C_s symmetry and ^6A electronic states of 12-XII.

So far we have explained the obtained geometries in the present work, and compared them to the available results of the previous calculations in Ref. [18]. We found different lowest-energy structures as G-S and some new isomers for small AlB_n (up to $n = 12$) since we have considered more structural isomers for each size. Furthermore, the $n = 13$ and 14 were also investigated. As shown in Fig. 11 the G-S isomer of AlB_{13} is in a 3D form, where the Al atom was adsorbed over the surface of quasi-planar boron atoms having 2-hexagonal pyramids as subunits. For this size, 16 isomers within the energy interval of 4.920 eV were considered but no planar configuration could be obtained as the G-S for the $n = 13$. The second low-lying energy structure is a quasi-planar (closer to planar orientation) which is 0.223 eV above the G-S structure. It has 4-hexagonal rings with one boron atom at their centers as subunits,

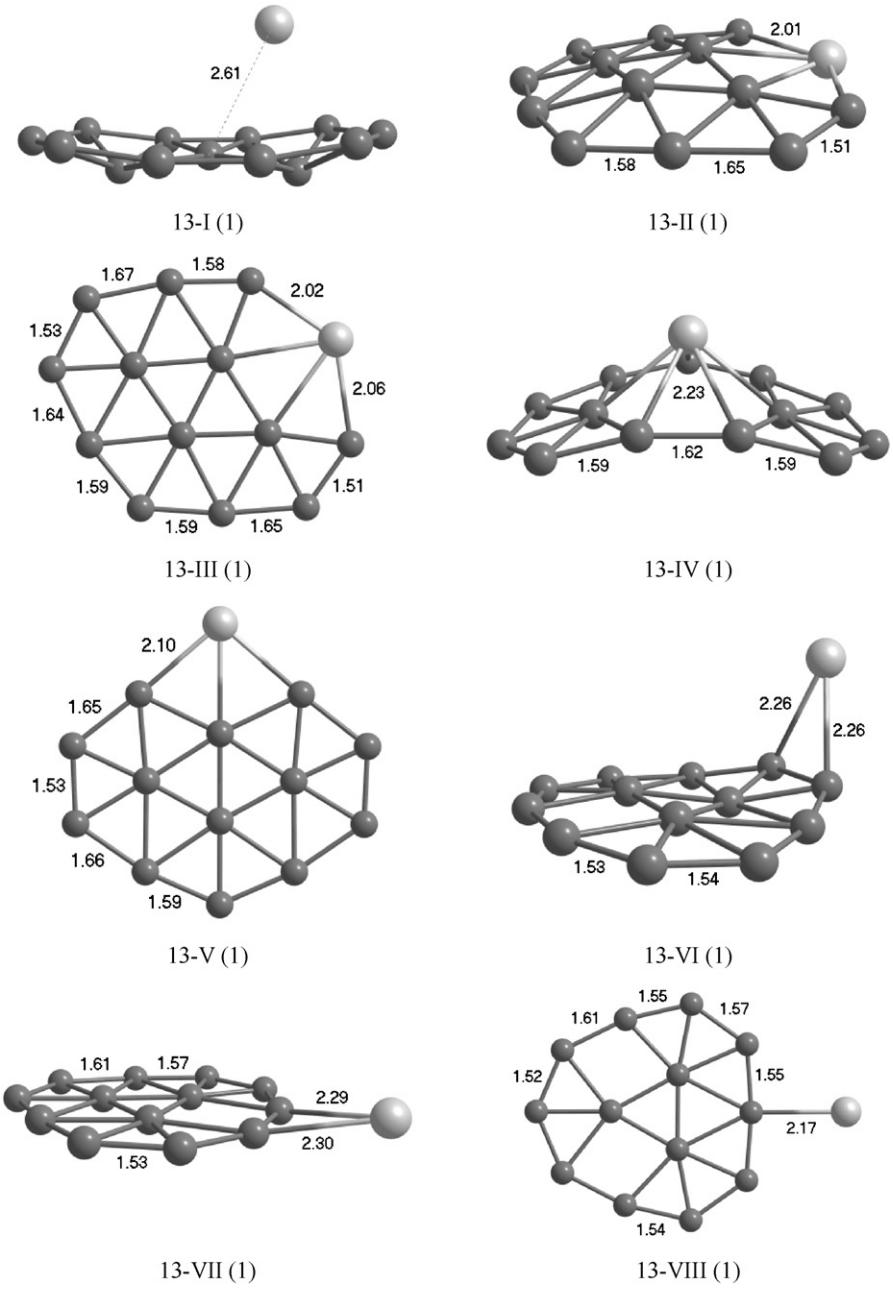

Fig. 11. Structures of AlB_{13} clusters.

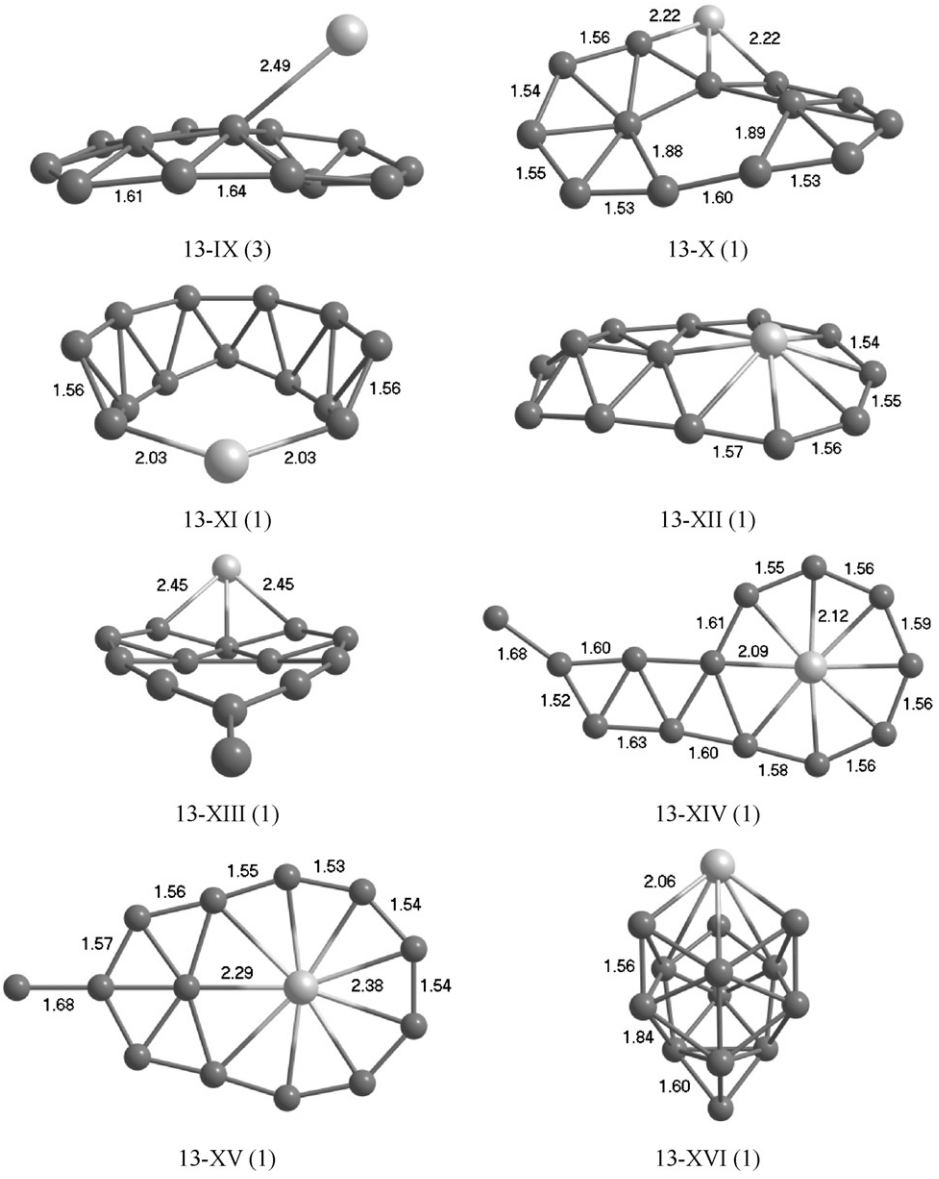

Fig. 11. (*Continued*).

in which the Al atom is a member of the outer 10-atom ring. Isomers 13-III, -V, -VII, -XIV and -XV are planar but energetically not lower than 13-I. The 3D structure, for example, the bowl-like one is the fourth stable isomer. Moreover, it is clear that the least stable isomer (13-XVI) is in a 3D cage form. As a result, the 3D structures are not more stable than the planar and quasi-planar geometries.

Twelve isomers within the energy interval of 5.940 eV for AlB_{14} are demonstrated in Fig. 12. Mainly the low-lying stable structures are in 2D planar forms. The G-S structure is in a semi planar form however, it is almost planar. Isomer 14-I and its little distorted form 14-II have one hexagonal and 3-heptagonal connected rings with one boron atom at their centers. One of the heptagonal rings has the Al atom. The third low-lying energy structure, 14-III, has Al-membered one hexagonal and 3-heptagonal connected rings with one boron atom at their centers in the same plane. The first 3D isomer in this group of $n = 14$ is 14-VI.

From the discussion above it is understood that substantial structural reconstruction is observed with Al doping and the relatively more stable structures are mainly in 2D configurations for AlB_n ($n = 1$–14). The G-S structures for $n = 6$ and $n = 13$ are quasi-planar but closer to planar forms. For $n = 8$ and $n = 13$ the G-S isomers are in 3D forms. It is found that in the lowest-energy structures, the Al atom favors either the outer side or above the surface of the clusters, not the center of the clusters, except for the AlB_9. The single dropped Al atom hardly affects the shape of the larger host boron clusters.

Further investigation may be conducted to demonstrate that the planar/quasi-planar metal-boron is relatively more stable than any 3D isomers in this size range. Moreover, increasing the value of spin multiplicity leads to less stable configurations (except for AlB dimmer).

The growing patterns of AlB_n ($n = 1$–14) clusters are illustrated in Fig. 13. The possible simple growth-path from the previous size to the next size is discussed below. This growth-path simply shows the least structural modifications on the clusters, as moved from one size to the next size. This path is emphasized by the drawn arrows within the figure. It should be pointed out that although the isomers can be called many different names to identify their structural appearances, we only categorize them in linear, planar, or cage and with their interphases as convex, quasi-planar, or open-cage

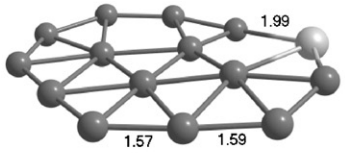

14-I (2)

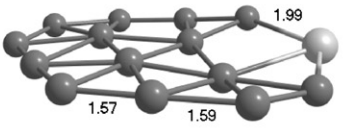

14-II (2)

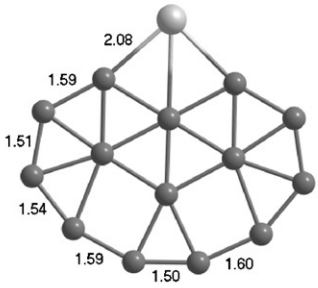

14-III (2)

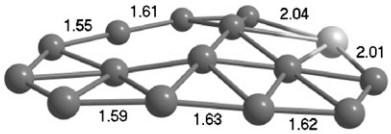

14-IV (2)

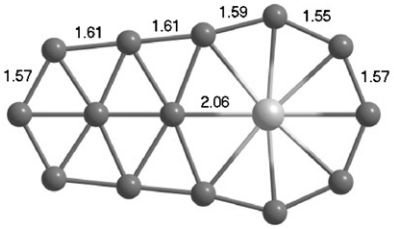

14-V (2)

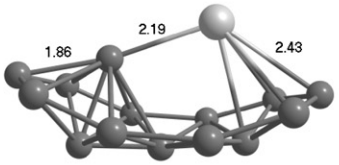

14-VI (2)

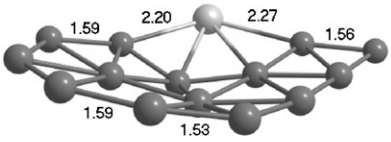

14-VII (2)

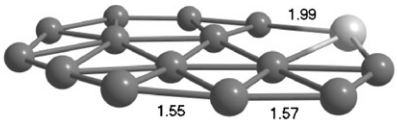

14-VIII (4)

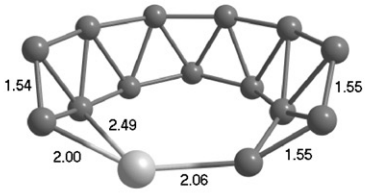

14-IX (2)

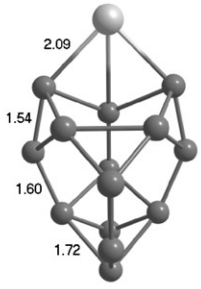

14-X (2)

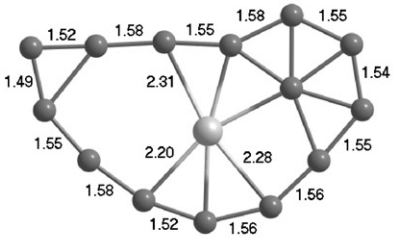

14-XI (2)

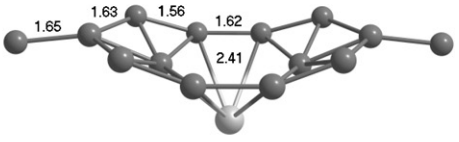

14-XII (2)

Fig. 12. Structures of AlB_{14} clusters.

configurations as sketched in Fig. 13. Clearly, AlB_2 grows with two possibilities from 2-atom AlB cluster namely to a triangular or to a linear structure. The linear structures are not energetically favorable isomers (as seen Fig. 1). Therefore, mainly the two and three dimensional structures are considered for the higher sizes. The simple growth-path of the most stable clusters will be discussed here. Energetically favored structures for the sizes of $n = 3$–5 in Fig. 13 follow planar forms. For the next size, AlB_6, the most stable isomer is in a quasi-planar geometry. It is in planar form for AlB_7 and in cage form for AlB_8. For the following sizes of $n = 9$–12 the planar configurations are energetically favored in the most stable isomers. Open cage (bowl-like) and quasi-planar forms are the most stable clusters for AlB_{13} and AlB_{14}.

Now atomization or binding energies will be examined to probe the stability of the considered clusters. The average binding energies per atom for AlB_n are compared with the previous results in Fig. 14. It can be observed that the binding energy essentially decreases sharply for very small clusters and then follows smoothly with increasing cluster size. This means that the clusters gain energy during the growth process which is in agreement with Ref. [18]. The evaluation of the average binding energies per atom is nearly parallel for both Al-doped and pure boron cases. The energies of the AlB_n clusters are higher than those of the pure B_n clusters (except for AlB dimmer). This demonstrates that the doping of Al atom does not improve the stability of boron clusters. Similar to Ref. [18] all the curves reveal almost the same size dependence indicating the relation between the stabilities of AlB_n and of pure B_n.

The dissociation energies of B and Al atoms from the AlB_n clusters are plotted in Figs. 15 and 16, respectively. They were calculated with Eqs. (2) and (3). The separation energy interval for a B atom is between 4.0 and 6.5 eV (Fig. 15). It is between 1.5 and 3.5 eV for the Al atom (Fig. 16). This demonstrates that AlB_n clusters form higher stability environments for the B atom rather than for the Al atom. Trends of the dissociation energies of bare boron clusters and AlB_n are similar and both of them go through large fluctuations within the energy range of 4.5–6.5 eV. Behaviors in the smaller size range are different because the influence of the Al atom is more appreciable. The lowest value is calculated for $n = 12$, indicating that AlB_{11} is more stable compared to the neighboring sizes. Moreover, as seen in Fig. 15 the adsorption energies show local maxima at $n = 3$, 5, 8, 11, and 13, and local minima at $n = 2$, 4, 10, 12, 14. This indicates that the Al-doped boron clusters of $n = 3$, 5, 8, 11, and 13 display more resistance than those

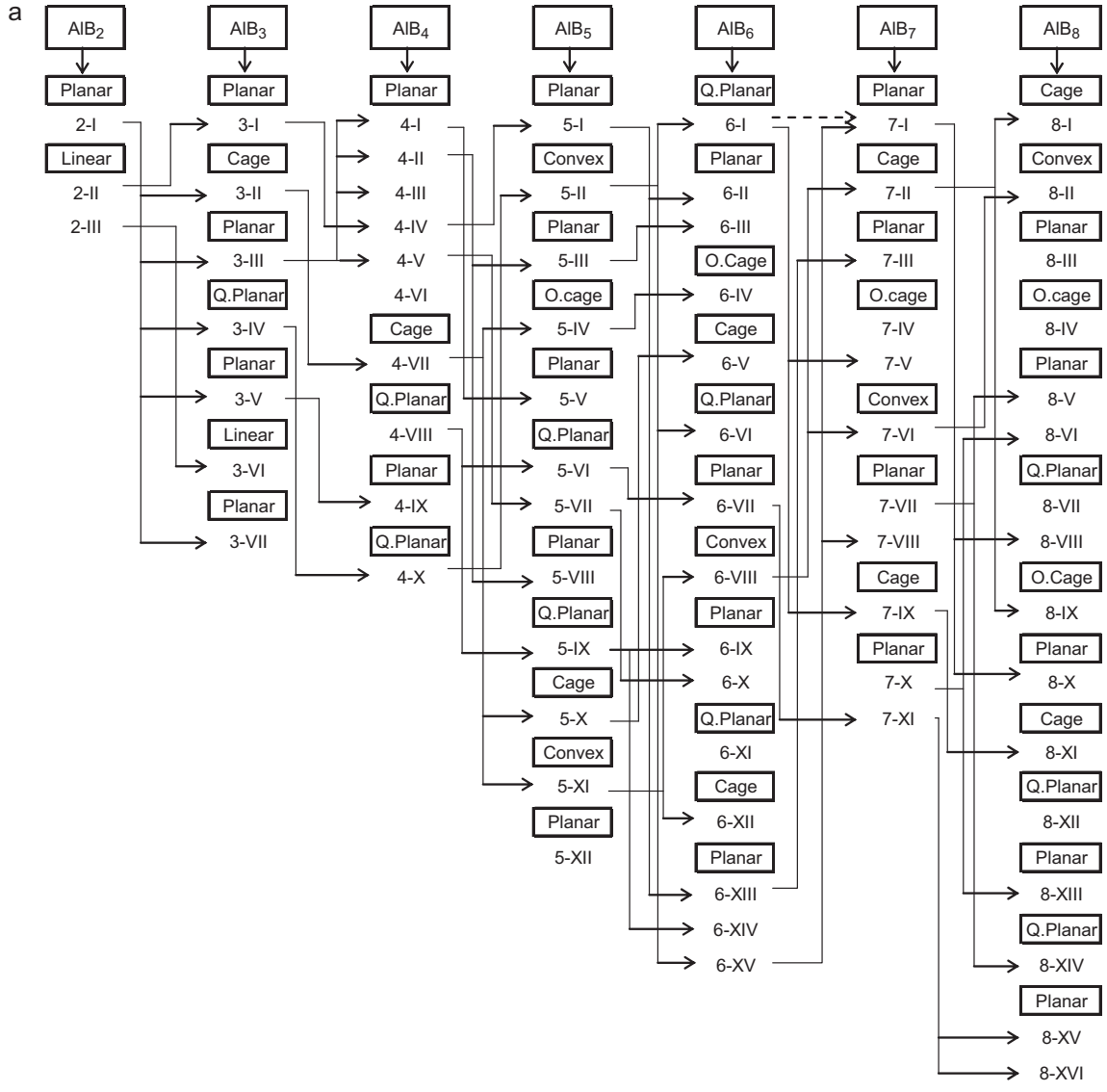

Fig. 13. Growing patterns of AlB_n ($n = 1$–14) clusters.

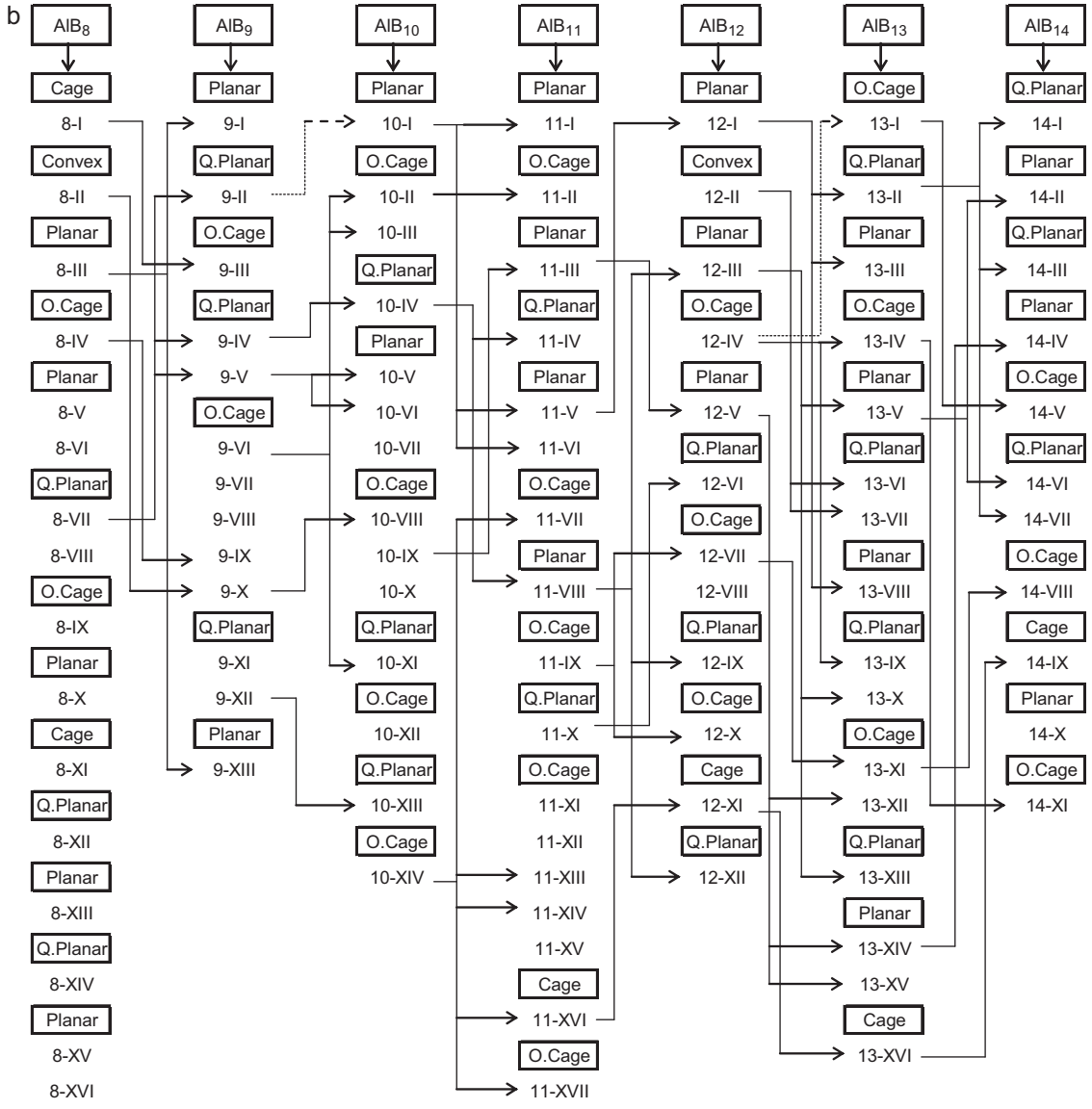

Fig. 13. (*Continued*).

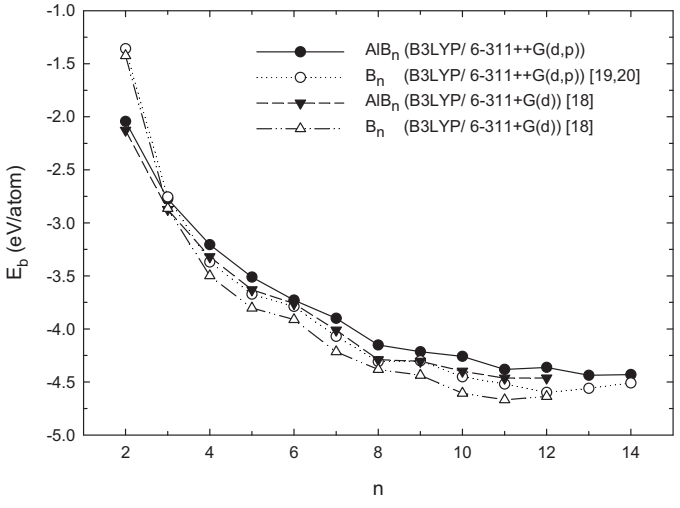

Fig. 14. Binding energy per atom of AlB_n and B_n clusters.

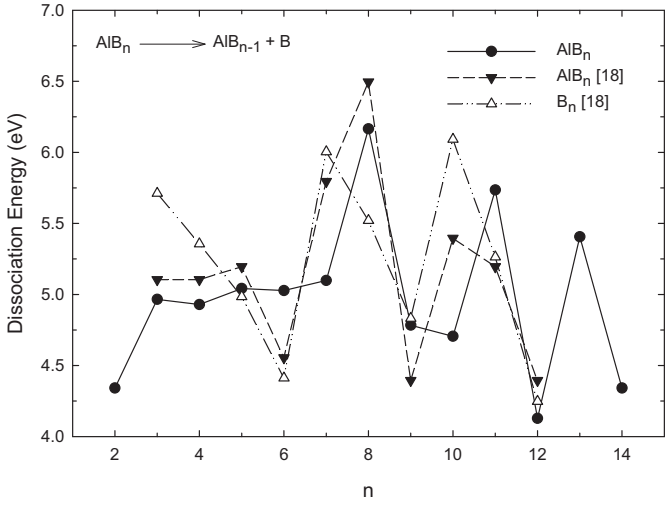

Fig. 15. Dissociation energy of B atom of AlB_n and B_n clusters.

Table 1
Calculated spin multiplicity (s), point group (PG), electronic states (ES), shortest Al–B (R_{Al-B} (Å)) and B–B (R_{B-B} (Å)) bond lengths, total energies (E_{tot} (eV)), total energies difference (ΔE (eV)), bond energies (E_b (eV)), HOMO–LUMO energy gap (gap_{HL} (eV)), atomic charges of Al atom (charge), minimum (f_{min}) and maximum (f_{max}) values of frequencies for (AlB_n) (n = 1–14) by using the B3LYP/6-311++g** level of DFT (Number of negative frequencies are given in the superscripted parenthesis over f_{min}).

Iso	PG	ES	R_{Al-B} (Å)	R_{B-B} (Å)	E_{tot} (eV)	ΔE (eV)	E_b (eV/at)	gap_{HL} (eV)	Charge	f_{min} (cm^{-1})	f_{max} (cm^{-1})
1-I	$C_{\infty V}$	$^3\Sigma$	2.050		−7268.617	0	0.895	1.789	0.254	585	
2-I	C_{2V}	$^2A'$	2.024	1.553	−7944.064	0	2.044	2.308	0.359	522	1051
2-II	C_S	$^4A''$	1.962	1.507	−7943.032	1.032	1.700	2.963	0.717	122	1336
2-III	C_S	$^4A''$	2.056	4.279	−7941.099	2.965	1.056	2.021	−0.069	$438^{(1)}$	486
3-I	C_S	^1A	2.188	1.516	−8620.135	0	2.774	2.604	0.387	102	1275
3-II	C_S	^1A	2.536	1.537	−8619.990	0.145	2.738	3.056	0.377	89	1256
3-III	C_{2V}	^1A	1.997	1.524	−8619.753	0.382	2.679	1.983	0.265	238	1232
3-IV	C_S	^5A	2.085	1.645	−8618.586	1.549	2.387	2.987	0.390	149	1032
3-V	C_S	^1A	2.057	1.515	−8616.558	3.577	1.880	1.961	0.215	76	1192
3-VI	C_{8V}	^7A	1.949	1.539	−8616.081	4.054	1.761	3.403	0.175	95	1271
3-VII	C_S	^3A	2.075	3.450	−8613.845	6.290	1.202	1.994	−0.003	$21^{(2)}$	570
4-I	C_S	^2A	2.042	1.535	−9296.169	0	3.205	3.115	0.417	208	1310
4-II	C_S	^2A	2.055	1.532	−9296.061	0.108	3.184	3.267	0.366	$194^{(1)}$	1317
4-III	C_S	^2A	2.140	1.546	−9296.013	0.156	3.174	3.263	0.303	99	1223
4-IV	C_S	^2A	2.149	1.554	−9295.998	0.171	3.171	2.514	0.530	79	1167
4-V	C_S	^2A	2.023	1.544	−9295.616	0.553	3.095	2.653	0.262	226	1243
4-VI	C_{2V}	^2A	2.045	1.543	−9295.262	0.907	3.024	2.244	0.301	128	1372
4-VII	C_S	^2A	2.123	1.569	−9294.718	1.451	2.915	2.701	0.379	$280^{(1)}$	1147
4-VIII	C_2	^4A	2.201	1.554	−9294.439	1.730	2.859	1.909	0.299	140	1353
4-IX	C_S	^2A	2.136	1.536	−9291.483	4.686	2.268	1.875	0.061	87	1170
4-X	C_S	^8A	2.148	1.588	−9290.206	5.963	2.013	2.348	0.180	116	1063
5-I	C_S	^1A	2.207	1.542	−9972.317	0	3.511	1.966	0.426	83	1332
5-II	C_S	^1A	2.230	1.578	−9972.190	0.127	3.490	3.077	0.195	216	1191
5-III	C_S	^1A	2.100	1.546	−9971.462	0.855	3.369	2.181	0.467	$74^{(2)}$	1356
5-IV	C_S	^3A	2.111	1.571	−9970.796	1.521	3.258	2.331	0.295	215	1201
5-V	C_S	^5A	2.055	1.532	−9970.744	1.573	3.249	2.670	0.536	167	1240
5-VI	C_S	^1A	2.024	1.531	−9970.609	1.708	3.227	1.561	0.335	159	1351
5-VII	C_S	^1A	2.008	1.523	−9970.515	1.802	3.211	1.408	0.459	118	1297
5-VIII	C_S	^5A	2.086	1.576	−9970.460	1.857	3.202	3.336	0.856	$125^{(1)}$	1272
5-IX	C_S	^1A	2.032	1.535	−9970.301	2.016	3.176	1.229	0.423	82	1420
5-X	C_2	^1A	2.203	1.553	−9970.108	2.209	3.143	2.001	0.250	214	1168
5-XI	C_{5V}	^1A	2.128	1.603	−9969.579	2.738	3.055	1.258	0.251	$451^{(2)}$	1102
5-XII	C_S	^9A	2.218	1.538	−9966.319	5.998	2.512	2.163	0.429	55	1392
6-I	C_S	^2A	2.111	1.539	−10648.449	0	3.728	2.247	0.245	127	1257
6-II	C_S	^2A	2.147	1.525	−10647.976	0.473	3.660	1.976	0.541	49	1349
6-III	C_S	^2A	2.144	1.534	−10647.970	0.479	3.660	2.161	0.436	22	1351
6-IV	C_2	^2A	2.156	1.548	−10647.803	0.646	3.636	2.856	0.322	178	1208
6-V	C_S	^2A	2.255	1.594	−10647.793	0.656	3.634	2.354	0.235	142	1057
6-VI	C_S	^4A	2.150	1.547	−10647.230	1.219	3.554	2.060	0.537	$170^{(1)}$	1226
6-VII	C_S	^2A	2.017	1.481	−10647.064	1.385	3.530	2.599	0.117	107	1371
6-VIII	C_2	^2A	2.300	1.556	−10646.989	1.460	3.519	2.024	0.343	234	1318
6-IX	C_S	^2A	2.021	1.493	−10646.879	1.570	3.504	2.424	−0.195	86	1473
6-X	C_S	^2A	2.008	1.491	−10646.751	1.698	3.485	1.814	0.341	72	1434
6-XI	C_S	^2A	2.180	1.557	−10646.732	1.717	3.483	1.934	0.241	$56^{(1)}$	1268
6-XII	C_S	^4A	2.187	1.640	−10646.654	1.795	3.472	2.459	0.424	168	1007
6-XIII	C_S	^2A	2.159	1.556	−10646.600	1.849	3.464	2.179	0.602	40	1307
6-XIV	C_S	^4A	2.164	1.533	−10646.191	2.258	3.405	2.054	0.014	124	1490
6-XV	C_S	^6A	2.059	1.560	−10645.906	2.543	3.365	3.546	0.546	206	1291
6-XV	C_S	^6A	2.059	1.560	−10645.906	2.543	3.365	3.546	0.546	206	1291
7-I	C_S	^1A	2.032	1.500	−11324.653	0	3.899	1.525	0.504	138	1488
7-II	C_S	^1A	2.479	1.543	−11324.479	0.174	3.878	2.078	0.495	135	1239
7-III	C_S	^1A	2.133	1.490	−11324.071	0.582	3.827	1.612	0.599	58	1408
7-IV	C_S	^1A	2.083	1.520	−11324.048	0.605	3.824	2.640	0.221	152	1252
7-V	C_S	^1A	2.207	1.570	−11323.828	0.825	3.796	2.540	0.403	41	1144
7-VI	C_S	^1A	2.137	1.533	−11323.646	1.007	3.774	1.916	0.248	14	1332
7-VII	C_S	^1A	2.022	1.499	−11323.626	1.027	3.771	1.219	0.712	96	1338
7-VIII	C_S	^5A	2.103	1.584	−11323.543	1.110	3.761	3.629	1.376	53	1187
7-IX	C_S	^1A	2.032	1.541	−11323.541	1.112	3.760	2.015	0.310	230	1254
7-X	C_S	^1A	1.973	1.500	−11323.540	1.113	3.760	1.249	1.199	92	1326
7-XI	C_S	^1A	1.980	1.498	−11323.359	1.294	3.738	2.420	0.270	128	1422
8-I	C_S	^2A	2.121	1.543	−12001.923	0	4.151	5.383	0.728	145	1400
8-II	C_2	^2A	2.162	1.550	−12000.804	1.119	4.027	3.501	0.160	102	1459
8-III	C_S	$^2A''$	2.078	1.574	−12000.517	1.406	3.995	3.610	−0.580	$276^{(2)}$	1348
8-IV	C_S	^2A	2.067	1.537	−12000.297	1.626	3.970	2.139	0.162	157	1251
8-V	C_S	^2A	2.126	1.517	−12000.275	1.648	3.968	2.264	0.251	66	1381
8-VI	C_S	^2A	1.994	1.517	−12000.149	1.774	3.954	2.381	0.670	77	1405
8-VII	C_S	^2A	2.112	1.570	−11999.910	2.013	3.927	2.634	0.291	142	1246
8-VIII	C_S	^2A	1.958	1.514	−11999.706	2.217	3.905	2.452	0.850	53	1568
8-IX	C_S	^4A	2.258	1.557	−11999.700	2.223	3.904	3.148	0.777	149	1228
8-X	C_S	^2A	1.961	1.499	−11999.652	2.271	3.899	2.187	0.746	$102^{(1)}$	1640
8-XI	C_S	^2A	2.065	1.543	−11999.312	2.611	3.861	2.500	0.367	202	1213
8-XII	C_S	^2A	2.104	1.540	−11999.310	2.613	3.861	2.497	0.152	137	1341
8-XIII	C_S	^2A	2.081	1.520	−11999.284	2.639	3.858	2.157	1.112	64	1357
8-XIV	C_S	^2A	2.034	1.514	−11999.261	2.662	3.855	2.157	0.166	123	1380

Table 1 (*Continued*)

Iso	PG	ES	R_{Al-B} (Å)	R_{B-B} (Å)	E_{tot} (eV)	ΔE (eV)	E_b (eV/at)	gap_{HL} (eV)	Charge	f_{min} (cm^{-1})	f_{max} (cm^{-1})
8-XV	C_S	^2A	2.050	1.540	−11999.190	2.733	3.847	1.931	0.419	92	1411
8-XVI	C_2	^2A	1.991	1.514	−11998.055	3.868	3.721	1.719	0.065	34(1)	1393
9-I	C_S	$^1A'$	2.253	1.542	−12677.812	0	4.214	3.263	−0.443	129	1567
9-II	C_S	^1A	2.060	1.544	−12677.526	0.286	4.186	2.278	0.357	123	1312
9-III	C_S	^1A	2.496	1.514	−12677.409	0.403	4.174	4.545	0.436	17	1678
9-IV	C_2	^1A	2.038	1.549	−12677.310	0.502	4.164	2.179	0.353	130	1318
9-V	C_S	^1A	2.054	1.564	−12677.246	0.566	4.158	3.023	0.336	105	1295
9-VI	C_S	^1A	2.482	1.556	−12676.637	1.175	4.097	2.411	0.713	136	1279
9-VII	C_S	^1A	2.250	1.566	−12676.093	1.719	4.042	2.194	0.331	60	1222
9-VIII	C_S	^1A	2.242	1.553	−12676.072	1.740	4.040	2.515	0.246	59	1249
9-IX	C_S	^1A	2.015	1.526	−12675.813	1.999	4.014	2.447	0.265	67	1253
9-X	C_S	^1A	2.370	1.504	−12674.642	3.170	3.897	1.774	0.342	67	1551
9-XI	C_2	^1A	2.288	1.513	−12674.626	3.186	3.896	2.470	0.205	68	1348
9-XII	C_2	^1A	2.195	1.518	−12674.121	3.691	3.845	1.576	0.095	119(1)	1345
9-XIII	C_S	$^5A'$	2.290	1.566	−12674.038	3.774	3.837	1.197	−0.333	82	1448
10-I	C_S	^2A	2.037	1.516	−13353.623	0	4.259	2.875	0.728	67	1552
10-II	C_S	^2A	2.714	1.575	−13353.612	0.011	4.258	2.881	0.624	94	1311
10-III	C_S	^2A	2.316	1.571	−13353.476	0.147	4.246	3.219	0.166	42	1262
10-IV	C_2	^2A	1.969	1.516	−13353.133	0.490	4.214	2.767	0.367	113	1527
10-V	C_S	^2A	1.993	1.526	−13353.084	0.539	4.210	2.349	0.832	116	1545
10-VI	C_S	^2A	2.000	1.525	−13353.082	0.541	4.210	2.350	0.783	114(1)	1539
10-VII	C_S	^2A	2.163	1.534	−13353.047	0.576	4.207	2.509	0.730	46	1477
10-VIII	C_S	^2A	2.480	1.524	−13352.671	0.952	4.172	2.851	0.376	89	1514
10-IX	C_S	^2A	1.999	1.550	−13352.451	1.172	4.152	2.780	−0.067	143	1401
10-X	C_S	^2A	2.060	1.565	−13352.223	1.400	4.132	3.201	0.330	50	1254
10-XI	C_S	^4A	2.149	1.561	−13352.203	1.420	4.130	2.311	0.235	95	1252
10-XII	C_S	^2A	2.067	1.538	−13351.761	1.862	4.090	2.543	0.467	85	1328
10-XIII	C_S	^2A	2.172	1.518	−13349.968	3.655	3.927	2.240	−0.480	99	1344
10-XIV	C_5	^2A	2.204	1.652	−13349.244	4.379	3.861	2.582	0.445	261	1031
11-I	C_S	^1A	2.218	1.538	−14030.464	0	4.382	3.110	0.611	29	1478
11-II	C_S	^1A	2.661	1.530	−14029.764	0.700	4.324	2.465	0.575	62	1505
11-III	C_S	^1A	2.040	1.543	−14029.268	1.196	4.282	2.041	−0.711	148(1)	1412
11-IV	C_S	^3A	2.127	1.531	−14029.022	1.442	4.262	1.503	0.200	101	1422
11-V	C_S	^1A	2.077	1.514	−14028.511	1.953	4.219	2.104	0.538	42	1589
11-VI	C_S	^1A	2.011	1.509	−14028.393	2.071	4.210	2.533	0.894	75	1558
11-VII	C_S	^1A	2.100	1.615	−14028.257	2.207	4.198	2.791	0.073	142	1145
11-VIII	C_S	^1A	1.967	1.524	−14028.252	2.212	4.198	2.212	0.140	86	1441
11-IX	C_S	^1A	2.015	1.545	−14028.173	2.291	4.191	2.433	0.253	57	1271
11-X	C_S	^5A	2.215	1.548	−14027.741	2.723	4.155	2.819	0.484	84	1405
11-XI	C_S	^1A	2.524	1.577	−14027.488	2.976	4.134	3.167	0.540	106	1191
11-XII	C_S	^1A	2.353	1.603	−14027.432	3.032	4.129	1.895	0.568	89	1155
11-XIII	C_S	$^1A'$	2.092	1.559	−14027.161	3.303	4.107	1.762	0.542	121(1)	1262
11-XIV	C_S	^1A	2.220	1.578	−14026.996	3.468	4.093	2.511	0.047	185	1167
11-XV	C_S	^1A	2.167	1.573	−14026.953	3.511	4.089	1.908	0.006	150	1211
11-XVI	C_{5V}	^1A	2.497	1.644	−14026.622	3.842	4.062	2.120	0.354	186	1026
11-XVII	C_S	^1A	2.434	1.575	−14026.510	3.954	4.053	2.070	0.251	65	1154
12-I	C_S	^2A	1.978	1.501	−14705.698	0	4.363	1.694	0.631	94	1528
12-II	C_S	^2A	2.185	1.552	−14705.679	0.019	4.361	1.915	0.190	30	1316
12-III	C_S	^2A	2.201	1.520	−14705.283	0.415	4.331	1.556	0.549	70	1534
12-IV	C_S	^2A	2.094	1.569	−14705.111	0.587	4.317	2.854	1.346	129	1376
12-V	C_S	$^2A''$	2.256	1.527	−14704.912	0.786	4.302	1.389	−0.349	76	1570
12-VI	C_S	^2A	2.216	1.513	−14704.528	1.170	4.273	2.382	0.242	45	1577
12-VII	C_S	^2A	2.001	1.547	−14704.200	1.498	4.247	1.888	0.176	82	1316
12-VIII	C_S	^2A	2.013	1.539	−14704.086	1.612	4.239	2.480	−0.056	131	1441
12-IX	C_S	^4A	2.048	1.523	−14703.772	1.926	4.215	2.074	0.616	84	1470
12-X	C_S	^2A	2.041	1.527	−14703.305	2.393	4.179	1.952	−0.057	67	1439
12-XI	C_S	^2A	2.111	1.584	−14702.852	2.846	4.144	2.226	0.425	231	1114
12-XII	C_S	^6A	2.078	1.544	−14701.928	3.770	4.073	2.180	0.505	84	1369
13-I	C_S	^1A	2.614	1.556	−15382.209	0	4.437	2.455	0.422	60	1307
13-II	C_S	^1A	2.012	1.507	−15381.986	0.223	4.421	2.301	0.440	82	1324
13-III	C_S	^1A	2.020	1.510	−15381.972	0.237	4.420	2.261	0.769	147(1)	1316
13-IV	C_S	^1A	2.216	1.540	−15381.685	0.524	4.400	2.239	1.162	95	1416
13-V	C_S	^1A	2.098	1.527	−15381.573	0.636	4.392	1.428	1.094	51(1)	1290
13-VI	C_S	^1A	2.256	1.525	−15381.521	0.688	4.388	1.416	0.315	43	1497
13-VII	C_S	^1A	2.295	1.512	−15381.429	0.780	4.381	1.654	0.702	57(1)	1474
13-VIII	C_S	^1A	2.173	1.518	−15381.342	0.867	4.375	1.325	0.761	17(2)	1457
13-IX	C_S	^3A	2.489	1.553	−15381.237	0.972	4.368	2.972	0.136	98	1261
13-X	C_2	^1A	2.219	1.526	−15380.839	1.370	4.339	1.751	−0.142	67	1555
13-XI	C_S	^1A	2.030	1.555	−15380.308	1.901	4.301	1.993	0.302	82	1331
13-XII	C_S	^1A	2.070	1.545	−15379.802	2.407	4.265	1.666	0.311	114	1480
13-XIII	C_S	^1A	2.262	1.548	−15378.863	3.346	4.198	1.191	0.095	41	1454
13-XIV	C_S	$^1A'$	2.056	1.519	−15377.704	4.505	4.115	1.615	−0.556	41(1)	1425
13-XV	C_{2V}	$^1A'$	2.225	1.531	−15377.651	4.558	4.112	1.322	−0.683	82(2)	1589
13-XVI	C_S	^1A	2.058	1.563	−15377.289	4.920	4.086	1.918	0.587	144	1154
14-I	C_S	^2A	1.982	1.507	−16057.656	0	4.431	1.542	0.370	82	1514
14-II	C_S	^2A	2.081	1.498	−16057.628	0.028	4.429	1.526	1.241	49(1)	1570
14-III	C_S	^2A	2.011	1.515	−16057.262	0.394	4.404	1.780	0.533	78	1468

Table 1 (*Continued*)

Iso	PG	ES	R_{Al-B} (Å)	R_{B-B} (Å)	E_{tot} (eV)	ΔE (eV)	E_b (eV/at)	gap_{HL} (eV)	Charge	f_{min} (cm^{-1})	f_{max} (cm^{-1})
14-IV	C_S	$^2A''$	2.057	1.555	−16057.222	0.434	4.402	1.777	−0.519	$86^{(2)}$	1439
14-V	C_S	^2A	2.191	1.543	−16057.196	0.460	4.400	2.742	0.614	97	1363
14-VI	C_S	^2A	2.201	1.526	−16056.945	0.711	4.383	2.110	−0.172	81	1484
14-VII	C_S	^4A	1.984	1.509	−16056.633	1.023	4.363	1.534	0.617	80	1513
14-VIII	C_S	^2A	1.996	1.540	−16056.419	1.237	4.348	1.924	−0.012	90	1330
14-IX	C_S	^2A	2.090	1.536	−16055.401	2.255	4.280	2.371	0.095	$154^{(1)}$	1325
14-X	C_S	$^2A''$	2.068	1.489	−16054.888	2.768	4.246	1.177	−1.212	$70^{(2)}$	1555
14-XI	C_S	^2A	2.147	1.559	−16051.716	5.940	4.035	1.921	0.108	12	1383

of $n = 2$, 4, 10, 12, 14 clusters for a boron atom separation. Similarly, the energies in Fig. 16 are the separation energies for the Al atom from the AlB_n cluster. Results indicates that the bare boron clusters of $n = 2$, 6, 9, 11, and 13 are more active and those of $n = 4$, 7, 10, 12, 14 are less active towards Al adsorption. Hence, one can conclude that the higher the clusters stability, the lower the reactivity, i.e., larger adsorption energy indicates that the formation of the Al-doped cluster is more favorable. The AlB_{11} and AlB_{13} are the common structures in Figs. 15 and 16 showing relatively more stable characteristics. However, AlB_9 seems more stable in Fig. 16 even though AlB_8 has the highest stability in Fig. 15. This is related to the AlB_9 configuration, in which the doped Al has bonds with all the boron atoms, centralized in the boron ring. Therefore, fragmentation of the B atom from AlB_9 is easier than fragmentation of the Al atom. As depicted in Fig. 15 there are significant differences between our findings and the reported values in Ref. [18] for single boron dissociations at $n = 6$, 7, 10 and 11. This is due to the fact that we found different isomers as the lowest-lying configurations of these sizes.

In order to elucidate the stability variation of different size clusters, the second-order difference of cluster energies are plotted as a function of the cluster size in Fig. 17. The pure B_n clusters are quite stable at $n = 5$, 8, 10, 12 in Refs. [19,20] and at $n = 5$, 8, 11 in Ref. [18], whereas they are relatively less stable at $n = 6$, 9, 11 (from Refs. [19,20]) and at $n = 6$, 9 11 in Ref. [18]. Thus, it is seen from the results of Refs. [18–20] that the adsorption energies of the boron clusters of $n = 5$, 8, 10, 11 and 12 look relatively quite smaller. From our findings maxima in Fig. 17 are found at $n = 8$, 11 and 13, for the AlB_n clusters, indicating that these clusters possess higher stability. Briefly, we can say the AlB_8 cluster has typical magic characteristic in the whole considered series of the clusters. This is in good agreement with Ref. [18]. Due to some differences of the present isomers (as the lowest-lying structures) there are clear differences between the computed values of the second-order energy differences of our results and those given in Ref. [18] (see Fig. 17).

Another useful way of examining the stability and the chemical reaction ability or hardness of the clusters is the HOMO–LUMO energy gaps of AlB_n calculated and compared with the other calculations in Fig. 18. There is not such a strong correlation between the HOMO–LUMO gaps and the energetic stability of the clusters. However, generally, the less reactive systems indicate the larger HOMO–LUMO gaps. For the AlB_n clusters, the local peaks from present computations are found at $n = 4$, 6, 8, 11, 13, implying the chemical stability of these clusters is relatively stronger than those of their neighbors. The energy gaps of AlB_n clusters are usually

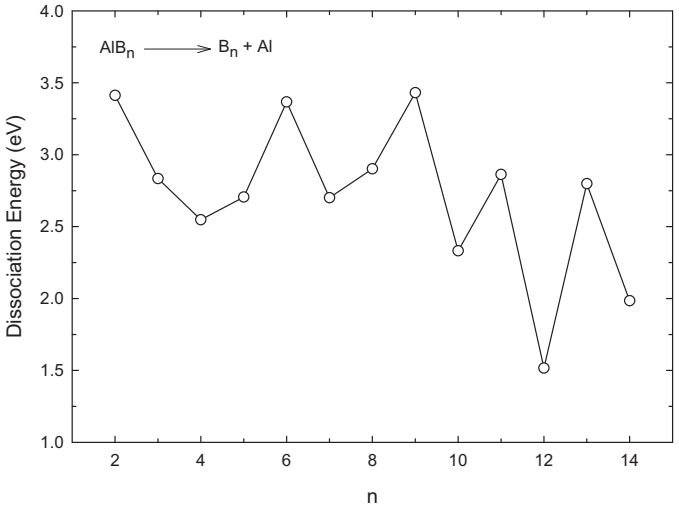

Fig. 16. Dissociation energy of Al atom of AlB_n clusters.

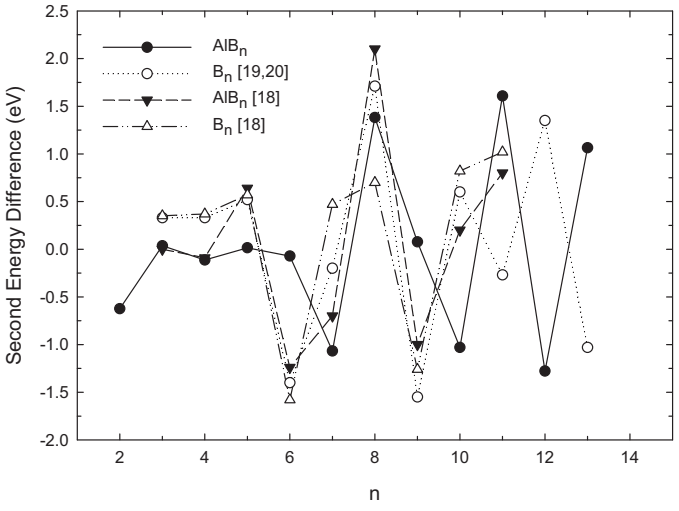

Fig. 17. Second energy differences of AlB_n and B_n clusters.

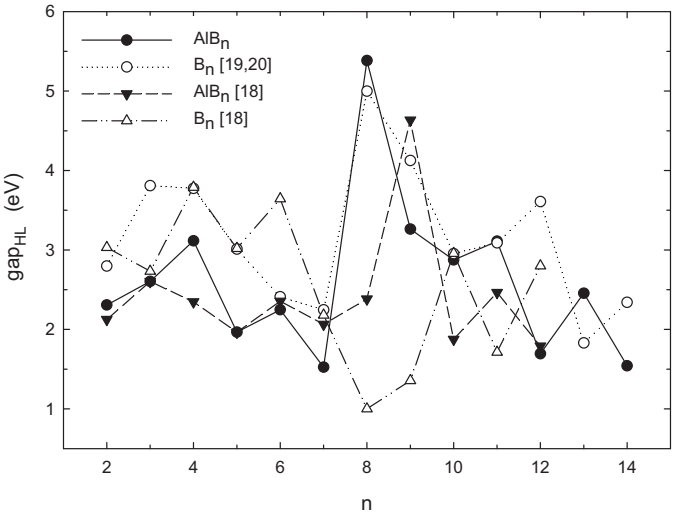

Fig. 18. HOMO–LUMO gap of AlB_n and B_n clusters.

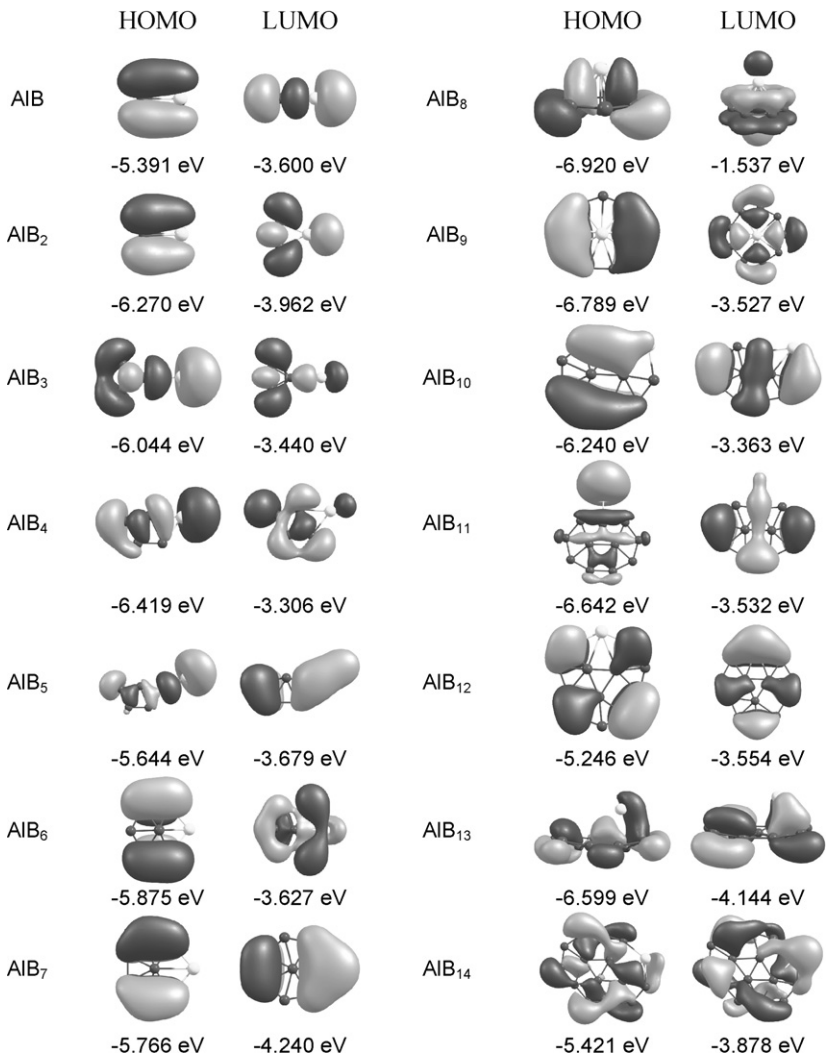

Fig. 19. HOMO and LUMO orbitals of AlB_n clusters.

smaller than those of B_{n+1} clusters (except at $n = 4$, 8, 9, 13) and those of B_n clusters (except at $n = 8$, 11, 13). It is expected that the magic clusters mostly have a very large HOMO–LUMO gap. It can be noted that the HOMO–LUMO gaps of AlB_n (for up to $n = 14$) present similar oscillating behaviors at $n = 8$, 11, and 13 as observed for the dissociation energy of B (Fig. 15) and for the second-order energy differences (Fig. 17). It is understood that these clusters are less reactive than the other clusters. The common structural properties of these AlB_8, AlB_{11} and AlB_{13} clusters are that the doped Al atom is out of the boron plate. That is, the boron atoms construct a grid among themselves via coming closer to each other while the Al atom is attached to them; in such configurations they exhibit stability. Finding new isomers as the lowest-lying energy configurations lead new HOMO–LUMO gaps which are different than those given in Ref. [18] for the same sizes. The gaps of AlB_8 are especially much different as seen in Fig. 18, however, the present G-S isomer of the AlB_8 is morphologically similar to the previously reported isomer in Ref. [18].

The HOMO and LUMO orbitals for the determined lower-lying isomers of the AlB_n clusters are demonstrated in Fig. 19. Since B and Al are in the same group of elements in the periodic table, they have strong hybridization between s and p orbitals. There are also degenerate orbitals depending on the size and configurations. The atomic charges of the Al atom of the G-S isomers of the AlB_n clusters are plotted in Fig. 20. The adsorption of the Al atom on boron clusters is governed by the charge-transfer process. Charge always transfers from the Al atom to the nearby B atoms. The big differences (compared to Ref. [18] for $n = 9$ and $n = 12$) are the results

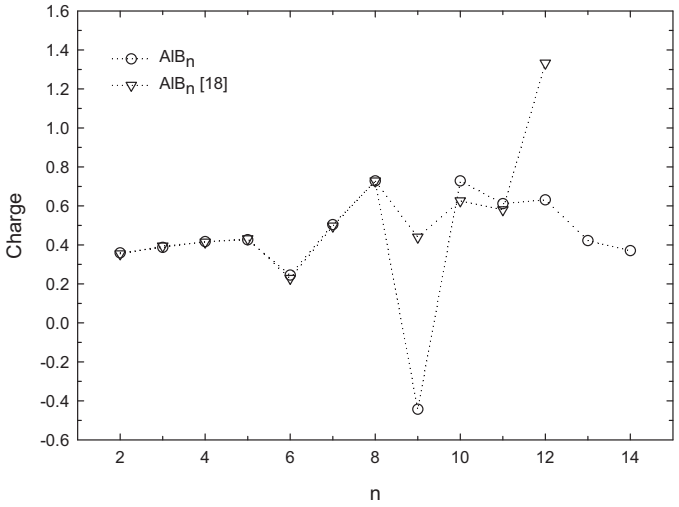

Fig. 20. Atomic charges of Al atom in AlB_n clusters.

of the big structural differences of the G-S isomers for these sizes. As the size increases Fig. 20 indicates that Al atom behaves as an electron donor in all G-S isomers of the AlB_n clusters, except in AlB_9. In all G-S structures the Al atom has positive charges, but in the AlB_9, it has a negative charge (its value is −0.44) since the configuration of the AlB_9 geometry is suitable for the charge flow from the B atoms to the Al atom. All boron atoms are positively charged in this isomer. Similarly, the wheel structure of 8-III isomer has negatively charged the Al atom which is at the center of B_8 ring as well. Moreover, any boron clusters containing an Al atom insight of the boron rings, similar to 8-III and 9-I, have charge transfer from the boron atoms, such as, 9-XIII, 10-IX, 11-III, 12-V, 13-XIV, 13-XV, 14-IV and 14-X. Some of the clusters, such as; 2-III, 3-VII, 6-XIV, 12-VIII have a negatively charged Al atom. In all such structures, the boron atoms are surrounding the Al atom. There are also a few structures that have a negatively charged Al atom, which are 10-XIII, 13-X and 14-VI (Al atom is at the substituting position of the quasi-planar forms of the AlB_{10}, AlB_{13} and AlB_{14}), 12-X and 14-VIII (Al atom is at the substituting position of the double ring of the clusters; AlB_{12} and AlB_{14}). Finally, in this particular study, it is clearly seen that the highest charge-transfer from the Al atom is observed in the G-S geometries of the AlB_8 and AlB_{10}. This means these clusters have high electrostatic interactions which makes them relatively more stable. The decrease in the charge-transfer in the sizes from $n = 12$ to $n = 14$ gives information about the loose of the electrostatic interaction effect.

Moreover, to analyze the size-dependent electronic stability of the G-S neutral clusters, the adiabatic ionization potential energy ($AIP(n) = E[AlB_n^+] - E[AlB_n]$) and the adiabatic electron affinity ($AEA(n) = E[AlB_n] - E[AlB_n^-]$) have been calculated and shown in Fig. 21(a) and (c). We have also calculated the vertical ionization potential (VIP) and vertical electron affinity (VEA) to determine the required energies to remove or add one electron on the G-S structures without any structural relaxation. Thus, the values of VIP and VEA were calculated as the energy differences of the neutral cluster from the corresponding positively charged cluster, and from the corresponding negatively charged cluster, respectively. Their calculated results are also plotted in Fig. 21(b) and (d). The first and second highest values of VIP are obtained for the AlB_9 and AlB_8 clusters, respectively. Relatively larger values appear for the AlB_4, AlB_6, AlB_9, AlB_{11} and AlB_{13} clusters. As we pointed out, the AlB_8, AlB_{11} and AlB_{13} have energetically high stability, called magic sizes. Although the VEA trend has abrupt changes for all the sizes, there are subsequently significant drops at $n = 3$, 5, 9 and 11. The low VEA should be related with their stabilities. However, the relation is not very clear. For example, AlB_9 and AlB_{11} have larger VIPs and relatively low VEAs. Similarly, AlB_{10} has relatively low VIP and the largest VEA. However, energetically stable clusters AlB_8 and AlB_{13} have large values for both VIPs and VEAs. These points may be examined in detail with future studies. Up to here, among all the studied clusters, AlB_8 and AlB_{13} are found as the magic-number in which the corresponding clusters have pronounced peaks for the binding energy, dissociation energy for boron, second-order energy differences, HOMO–LUMO gap and ionization potential, and electron affinity.

Fig. 22 shows the chemical hardness ($\eta \approx 1/2(I - A)$ where I is VIP and A is VEA). A chemically hard cluster should have a large HOMO–LUMO gap. This statement is, here, consistent with the maxima for $n = 8$, 11, 13 in Fig. 15 and the corresponding values in Fig. 22. However, the largest hardness value is observed for the AlB_9 in Fig. 22. This cluster has the second largest HOMO–LUMO gap. Another significant difference from the other sizes is the nega-

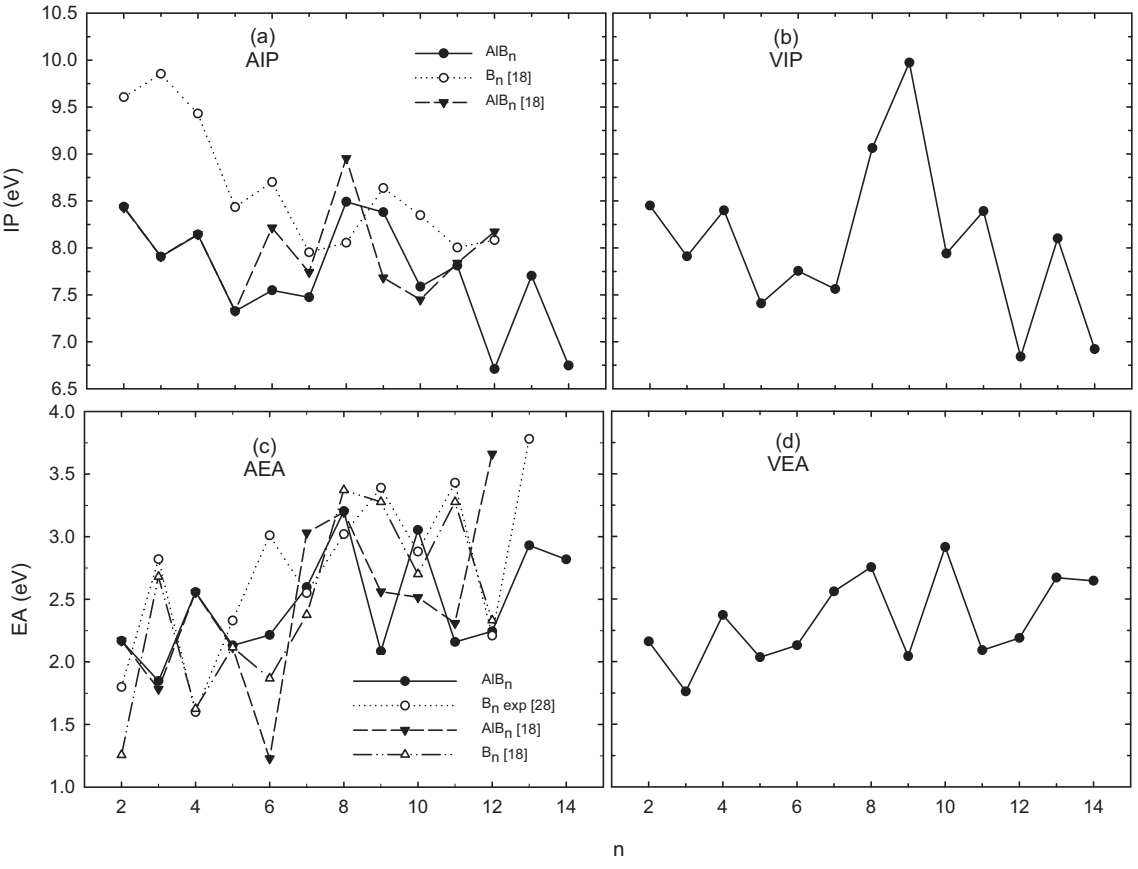

Fig. 21. AIP (a), AEA (b), VIP (c) and VEA (d) of AlB_n clusters.

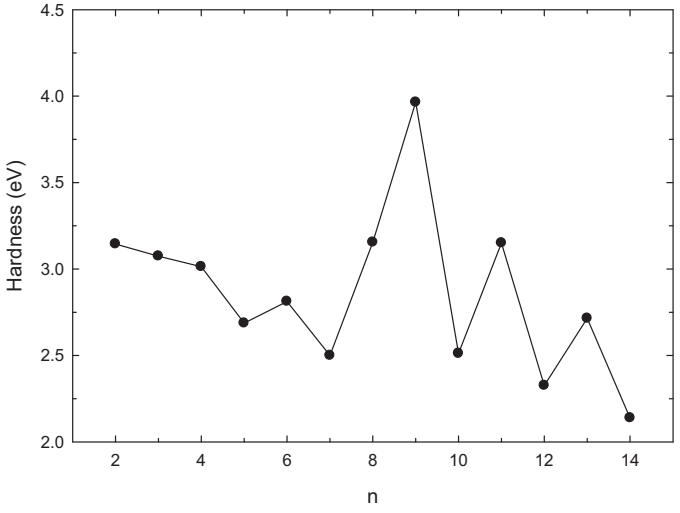

Fig. 22. Chemical hardness for AlB_n clusters.

tive charge collection on the Al atom centered in the cluster. It also agrees with the VIP values in Fig. 21(b).

4. Conclusion

A systematical DFT-B3LYP/6-311++G(d,p) investigation on the growth pattern, stability and electronic properties of the AlB_n clusters has been carried out with extensive calculations at $n = 1–14$. In boron clusters substantial structural reconstruction is observed with Al doping. A single doped Al atom hardly affects the shape of the host boron clusters. Increasing the value of spin multiplicity leads to less stable configurations (except for the AlB dimmer). It has been demonstrated that the relatively more stable structures are mainly in 2D configurations. The most stable structures for $n = 6$ and $n = 13$ are quasi-planar but closer to planar form. For $n = 8$ and $n = 13$ the G-S isomers are in 3D form. In the lowest-energy structures, the Al atom locates itself to the outer side and/or on the surface, not at the center of the cluster, except for the AlB_9. Further investigation may be needed to demonstrate that the planar/quasi-planar metal-boron is relatively more stable than any 3D isomers in this size range. The order of the structural stability may change with considering the ZPE correction. The results of the calculated first-order energy difference for a single boron atom dissociations and of the calculated second-order difference of energies show that the AlB_8, AlB_{11} and AlB_{13} clusters are the magic sizes, i.e., these clusters possess relatively high stability among the AlB_n clusters. The calculated first-order energy differences for the Al dissociations indicate that fragmentation of the Al atom from the structures at $n = 2$, 6, 7, 11 and 13 is relatively harder than the others. HOMO–LUMO gaps demonstrate the relatively higher chemical hardnesses at the AlB_8, AlB_{11} and AlB_{13} clusters. Moreover, ionization energy calculations show that AlB_9 also has chemical hardness.

Acknowledgement

This work was supported by TÜBİTAK (Grant No. 108T466) in part by Bozok University.

References

[1] A.I. Boldyrev, L.S. Wang, Chem. Rev. 105 (2005) 3716–3757.
[2] H. Haberland (Ed.), Clusters of Atoms and Molecules, Springer, Berlin, 1995.
[3] W.A. de Heer, Rev. Mod. Phys. 65 (1993) 611–676.
[4] Y. Gao, X.C. Zeng, J. Am. Chem. Soc. 127 (2005) 3698–3699.
[5] F. Baletto, R. Ferrando, Rev. Mod. Phys. 77 (2005) 371–423.
[6] M. Böyükata, Z.B. Güvenç, Braz. J. Phys. 36 (2006) 725–729.
[7] C.M. Chang, M.Y. Chou, Phys. Rev. Lett. 93 (2004) 133401.
[8] P. Calaminici, et al., J. Chem. Phys. 105 (1996) 9546–9556.
[9] L.G.M. Pettersson, C.W. Bauschlicher, T. Halicioğlu, J. Chem. Phys. 87 (1987) 2205–2213.
[10] T.H. Upton, J. Chem. Phys. 86 (1987) 7054–7064.
[11] J.G.O. Ojwang, R. Santen, G.J. Kramer, A.C.T. Duin, W.A. Goddard III, J. Chem. Phys. 129 (2008) 244506.
[12] A. Aguado, J.M. Lopez, J. Chem. Phys. 130 (2009) 064704.
[13] V.E. Oliker, V.L. Sirovatka, T.Y. Gridasova, I.I. Timofaeva, A.I. Bykov, Powder Metall. Met. Ceram. 47 (2008) 546–556.
[14] E. Finazzi, C.D. Valentin, G. Pacchioni, J. Phys. Chem. C 113 (2009) 220–228.
[15] I. Boustani, Phys. Rev. B 55 (1997) 16426–16438.
[16] Q.S. Li, L.F. Gong, Z.M. Gao, Chem. Phys. Lett. 390 (2004) 220–227.
[17] R. Linguerri, I. Navizet, P. Rosmus, S. Carter, J.P. Maier, J. Chem. Phys. 122 (2005) 034301.
[18] X.J. Feng, Y.H. Luo, J. Phys. Chem. A 111 (2007) 2420–2425.
[19] M. Atiş, C. Özdoğan, Z.B. Güvenç, Int. J. Quantum Chem. 107 (2007) 729–744.
[20] M. Atiş, C. Özdoğan, Z.B. Güvenç, Chin. J. Chem. Phys. 22 (2009) 380–388.
[21] X.J. Feng, Y.H. Luo, X. Liang, L.X. Zhao, T.T. Cao, J. Cluster Sci. 19 (2008) 421–433.
[22] M. Böyükata, C. Özdoğan, Z.B. Güvenç, Phys. Scripta 77 (2008) 025602.
[23] M. Böyükata, C. Özdoğan, Z.B. Güvenç, J. Mol. Struct.: Theochem. 805 (2007) 91–100.
[24] M. Böyükata, C. Özdoğan, Z.B. Güvenç, Rom. J. Inf. Sci. Technol. 11 (2008) 59–70.
[25] I. Yarovsky, A. Goldberg, Mol. Simulat. 31 (2005) 475–481.
[26] J. Jung, Y.–K. Han, J. Chem. Phys. 125 (2006) 064306.
[27] A. Goldberg, I. Yarovsky, Phys. Rev. B 75 (2007) 195403.
[28] H.J. Zhai, L.S. Wang, D.Y. Zubarev, A.I. Boldyrev, J. Phys. Chem. A 110 (2006) 1689–1693.
[29] Y. Zhi, Y.L. Yan, W.J. Zhao, X.L. Lei, G.X. Ge, Y.H. Luo, Acta Phys. Sin. 56 (2007) 2590–2595.
[30] M. Deshpande, D.G. Kanhere, R. Pandey, Phys. Rev. A 71 (2005) 063202.
[31] J.G. Yao, X.W. Wang, Y.X. Wang, Chem. Phys. 351 (2008) 1–6.
[32] X. Liu, G.F. Zhao, L.J. Guo, Q. Jing, Y.H. Luo, Phys. Rev. A 75 (2007) 063201.
[33] M.J. Frisch, et al., Gaussian 03, Revision D.01, 2004.